Microfluidics and Nanofluidics (2019) 23:116
https://doi.org/10.1007/s10404-019-2280-4

REVIEW

# A comprehensive review on liquid–liquid two-phase flow in microchannel: flow pattern and mass transfer

Jin-yuan Qian[1,2,3] · Xiao-juan Li[1] · Zan Wu[3] · Zhi-jiang Jin[1] · Bengt Sunden[3]

Received: 3 March 2019 / Accepted: 7 September 2019 / Published online: 24 September 2019


## Abstract

Liquid–liquid two-phase flow in microchannel is very common in micro-chemical and micro-biological system, etc. Deep understanding of the liquid–liquid two-phase flow mechanisms and mass transfer in microchannel can promote industrial applications significantly. To summarize the recent research progress on the liquid–liquid two-phase flow in microchannel, this paper collects research work about this topic, especially focusing on flow pattern and mass transfer. To begin with, flow patterns observed in various conditions are identified and factors which influence the flow patterns are analyzed. Then, mass transfer in liquid–liquid two-phase flow is discussed, especially the mass transfer during droplet flow, with both experiments and simulations. Furthermore, energy dissipation involved in liquid–liquid two-phase flow in microchannel is also briefly discussed. Finally, future needs are proposed for extending the researches on liquid–liquid two-phase flow and enlarging its application fields.

**Keywords** Flow pattern · Mass transfer efficiency · Energy dissipation · Liquid–liquid two-phase flow · Microchannel

### List of symbols

| | |
|---|---|
| $C$ | Concentration of solute |
| $C_i$ | Arbitrary node concentration of the scalar |
| $C_\sigma$ | Standard deviation |
| $\bar{C}$ | Concentration which the mixing is achieving at ideal condition |
| $\langle C \rangle$ | Statistical average value of the normalized concentration in the analyzed droplet |
| $C^*$ | Equilibrium concentration of solute |
| $Ca$ | Capillary number |
| $c_i$ | Constant, i = 1, 2,3, … |
| $d_h$ | Hydraulic diameter |
| $h$ | Channel depth or film thickness |
| $IOS$ | Intensity of segregation |
| $k_L a$ | Overall volumetric mass transfer coefficient |
| $l_d$ | Droplet length |
| $l_U$ | Droplet unit length |
| $MI$ | Mixing index |
| $N$ | Number of the nodes in the analyzed droplet |
| $Q_d$ | Flow rate of the dispersed phase |
| $Q_c$ | Flow rate of the continuous phase |
| $R$ | Radius of droplet cap |
| $Re$ | Reynolds number |
| $u_c$ | Velocity of the continuous phase |
| $u_d$ | Velocity of the dispersed phase |
| $v$ | Droplet velocity |
| $w_c$ | Continuous phase channel width |
| $w_d$ | Dispersed phase channel width |
| $We$ | Weber number |

### Greek symbols

| | |
|---|---|
| $\alpha$ | Dispersed phase length fraction |
| $\delta$ | Dimensionless surface roughness |
| $\varepsilon_d$ | Dispersed phase fraction |
| $\lambda$ | Viscosity ratio of the dispersed phase to the continuous phase |
| $\mu$ | Viscosity |
| $\theta$ | Contact angle |
| $\rho$ | Density |
| $\sigma$ | Interfacial tension |
| $\tau$ | Residence time |

✉ Jin-yuan Qian
qianjy@zju.edu.cn

[1] Institute of Process Equipment, College of Energy Engineering, Zhejiang University, Hangzhou 310027, People's Republic of China

[2] State Key Laboratory of Fluid Power and Mechatronic Systems, Zhejiang University, Hangzhou 310027, People's Republic of China

[3] Department of Energy Sciences, Lund University, PO Box 118, Lund 22100, Sweden

| | |
|---|---|
| $\Phi$ | Flow rate ratio of the dispersed phase to the continuous phase |
| $\Gamma$ | Ratio of channel depth to the continuous phase channel width |
| $\Lambda$ | Ratio of the dispersed phase channel width to the continuous channel width |
| $\Omega$ | Dimensionless interfacial tension |

**Subscripts**

| | |
|---|---|
| aqu | Aqueous phase |
| c | Continuous phase |
| d | Dispersed phase |
| IL | Ionic liquid |
| KS | Kerosene phase |
| MF | Moving film |
| org | Organic phase |
| SF | Stagnant film |
| WF | With fim |
| WOF | Without film |
| WS | Water phase |

## 1 Introduction

In recent decades, ever-growing attention has been paid to microfluidic systems due to their outstanding features such as smaller volume, higher security, easier controlling and superior heat and mass transfer performance. The most common two-phase flows in microfluidic systems are gas–liquid flow and liquid–liquid flow. There are widely used in chemical synthesis (Zhao et al. 2015a; Oelgemöller and Shvydkiv 2011; Yue 2018), biomedicine (Zheng et al. 2013; Lee et al. 2014; Cao et al. 2013; Murphy et al. 2017) and solvent extraction (Yun et al. 2011; Wang and Luo 2017). In micro-scale, surface tension is more dominating compared to inertia force and gravity. Depending on operating conditions, different flow regimes are observed such as bubbly flow, Taylor flow, slug–bubbly flow, slug–annular flow, churn flow and annular flow in gas–liquid two-phase flow system and droplet flow, slug flow, slug–drop flow, deformed interface flow, annular flow and parallel flow in liquid–liquid two-phase flow system (Kashid et al. 2011a). For precise control, many researches have been conducted to determine the optimal parameters of the microfluidic systems. These parameters can be mainly classified into two aspects: parameter optimization of microfluidic device which includes structure optimization and dimension optimization; parameter optimization of fluid flow which includes two-phase property optimization and two-phase velocity optimization.

For better guidance on future work of two-phase flow in micro-scale, many reviews are presented. Gu et al. (2011), Karadimitriou and Hassanizadeh (2012), Seemann et al. (2012) and Cate et al. (2015) gave detailed reviews on fabrication of micro-devices and presented the most common materials used in micro-devices. Seemann et al. (2012), Vladisavljevic et al. (2012), Lee et al. (2016) and Cai et al. (2017) summarized the most common structures of micro-devices. Christopher and Anna (2007) reviewed microfluidic methods for generating continuous drop streams. Shui et al. (2007) discussed the methods of controlling multiphase flow to generate drop (or bubble) or stratified interfaces between fluidic phases. Cristini and Tan (2004), Antony et al. (2014), Mao and Yang (2017) and Chen et al. (2018) gave comprehensive introductions of numerical methods and experimental methods which have been used to carry out two-phase flow in micro-scale. Kashid et al. (2011) and Sattari-Najafabadi et al. (2018) reviewed studies on both gas–liquid and liquid–liquid mass transfer in micro-scale. Operating conditions and geometry effects on mass transfer were discussed. Antony et al. (2014) also reviewed mass transfer in micro-scale, especially mass transfer in slug flow. Yao et al. (2018) presented a detailed review which aimed at ionic liquid systems in microchannels. The hydrodynamics, mass transfer and application are summarized in detail. Antony et al. (2014), Chinnov et al. (2015) and Zhu and Wang (2017) classified the two-phase flow patterns and pointed out the factors affecting the flow patterns. Moreover, Song et al. (2006) reviewed reactions that occur within segmented flows in microfluidic systems. Teh et al. (2008) presented methods for drop mixing and sorting. Ward and Fan (2015) summarized the enhancement methods of mixing in micro-scale. Applications of two-phase flow in micro-scale are summarized by Oelgemöller and Shvydkiv (2011), Cao et al. (2013), Murphy et al. (2017), Yun et al. (2011), Wang and Luo (2017), Yao et al. (2015) and Šalić et al. (2012).

Liquid–liquid two-phase flow holds an important status in microfluidic systems. This paper mainly focuses on the mechanism of liquid–liquid two-phase flow in microchannel and mass transfer in liquid–liquid two-phase flow in microchannel. First, flow patterns observed in various conditions are identified and factors which influenced the flow patterns are analyzed. Then, mass transfer in liquid–liquid two-phase flow is discussed, especially mass transfer in droplet flow. Both experiments and simulations are presented. In addition, energy dissipation involved in liquid–liquid two-phase flow in microchannels is only briefly concluded since there are less studies published. Finally, future needs are proposed for extending the research on liquid–liquid two-phase flow and enlarging its application fields.

**Table 1** Dimensionless numbers used in liquid–liquid two-phase flow

| Expressions | Remarks |
|---|---|
| $Ca = \frac{\mu u}{\sigma}$ | *Ca* represents the relative magnitude of viscous force to interfacial tension. In micro-scale, viscous force and interfacial tension are dominating and its makes *Ca* an important parameter for clarifying the mechanism of two-phase flow in micro-scale |
| $Re = \frac{\rho u d_h}{\mu}$ | *Re* represents relative magnitude of inertial force to viscous force. In micro-scale, fluid flow is usually laminar flow and *Re* is less than 1000 |
| $We = \frac{\rho u^2 d_h}{\sigma}$ | *We* represents the relative magnitude of inertial force to interfical tension |
| $\lambda = \frac{\mu_d}{\mu_c}$ | $\lambda$ represents the viscosity ratio of the dispersed phase to the continuous phase. $\lambda$ is related to fluid physical property. Viscosity of Newtonian and non-Newtonian fluid has totally different effect on two-phase flow patterns |
| $\Phi = \frac{Q_d}{Q_c}$ | $\Phi$ represents the flow rate ratio of the dispersed phase to the continuous phase and it is the easiest to change among all parameters |
| $\Lambda = \frac{w_d}{w_c}$<br>$\Gamma = \frac{h}{w_c}$ | $\Lambda$ and $\Gamma$ represent the ratio of the dispersed phase channel width to the continuous channel width and the ratio of channel depth to the continuous phase channel width, respectively. They reflect the microchannel geometry effect on two-phase flow in micro-scale. The subscripts d and c represent dispersed phase and continuous phase, respectively. It is worth noting that the microchannel always has a regular cross section, mostly the rectangular shape, when refers to $\Lambda$ and $\Gamma$ |

## 2 Fundamentals of liquid–liquid two-phase flow in microchannels

### 2.1 Dimensionless numbers

The characteristics of liquid–liquid two-phase flow are affected by the following dimensional and physical parameters: continuous phase channel width $w_c$ and dispersed phase channel width $w_d$, channel depth $h$, hydraulic diameter $d_h$, velocity of the continuous phase $u_c$ and dispersed phase $u_d$ (or flow rate of the continuous phase $Q_c$ and dispersed phase $Q_d$), viscosity of the continuous phase $\mu_c$ and dispersed phase $\mu_d$, density of the continuous phase $\rho_c$ and dispersed phase $\rho_d$ and interfacial tension $\sigma$. The subscripts c and d represent the continuous phase and dispersed phase, respectively. Dimensionless parameters, deduced from the aforementioned parameters, are commonly used for describing the liquid–liquid two-phase flow (Table 1).

### 2.2 Flow patterns and flow patterns map

Flow patterns are determined by the interaction of various forces including inertia force, gravity, viscosity force and surface tension. In micro-scale, continuous phase and dispersed phase interact with each other in microchannels. Surface tension is more dominating and it makes liquid–liquid two-phase flow in microchannel more controllable. Two-phase interface varies with operating conditions and fluid properties; thus, various flow patterns are presented accordingly. Garstecki et al. (2006; De Menech et al. 2008) described forces which involved the droplet formation process in detail and identified three distinct regimes, namely squeezing, dripping and jetting to describe the droplet formation process. Xu et al. (2008) also distinguished the droplet formation mechanisms into three regimes as squeezing, transition and dripping. Later, the squeezing regime and dripping regime are often used by many researchers (Gupta and Kumar 2010a; He et al. 2010; Wehking et al. 2014; Van Loo et al. 2016). In the squeezing regime, the droplet formation process is mainly dominated by the buildup of pressure upstream of an emerging droplet. Droplet length is larger than the microchannel width. In this regime, flow pattern is slug flow dominated. In dripping regime, droplet formation process is mainly dominated by the shear stress which is exerted on the droplet tips. Generally, the droplet length in the dripping regime is smaller than microchannel width. In this regime, flow pattern is droplet flow. Both slug flow and droplet flow are more stable flow patterns than other flow patterns. Flow patterns which have been observed so far are summarized and presented in Table 2 and Fig. 1.

#### 2.2.1 Flow patterns in different conditions

Flow patterns depend on the microchannel geometries, property of two phases and flow rate of two phases. Many researches have been conducted for identifying the flow patterns under different conditions. Recent progress is summarized as follows.

1. Effect of microchannel features on flow patterns

For a given two-phase system, microchannel features including microchannel material, microchannel geometry both have great influence on flow patterns.

The most common materials for fabricating a microchannel are PTFE, PDMS, PMMA, glass and quartz. Effect of materials on flow patterns is mainly caused by the differences of wetting properties of the phases to the walls, namely the contact angle between phases and walls. The value of the contact angle is determined by phase properties and microchannel material. Salim et al. (2008) measured contact angles of oil droplets on quartz and glass of 12° and 3°, respectively. However, contact angles of water droplets were 42° and 38°, respectively. Table 3 shows the

**Table 2** A summary of flow patterns in published literature

| Ref. | Microchannel features (material; structure; dimension/μm) | Continuous phase–dispersed phase system; flow condition | Parameters varied | Flow patterns |
|---|---|---|---|---|
| Wehking et al. (2014) | PDMS; T-junction; $h=100$, $w_c \times w_d = 111\times55.5$, $150\times75$, $200\times100$, $250\times125$, $300\times150$ | Silicone oil–water; silicone oil–FC-43; silicone oil–aqueous solution with Alumina-oxide particles; $Q=100$–$9000$ μL/h | Viscosity of two phases, interfacial tension, microchannel dimensions | Droplet flow in T-junction, droplet flow in channel, parallel flow |
| Zhao et al. (2006) | PMMA; T-junction; $h\times w=600\times300$ | Water–kerosene; $u_{aqu}=9.26\times10^{-4}$–1.85 m/s, $u_{org}=9.26\times10^{-4}$–2.78 m/s | Velocities of two phases | Slug flow, monodispersed droplet flow, parallel flow with smooth interface and wavy interface, droplet populations, chaotic thin striations flow |
| Xu et al. (2006) | PMMA; T-junction with embedded quartzose capillary; $h\times w=150\times200$, $d_i=40$ | SDS–n-octane; $Q_{aqu}=30$–$500$ μml/min, $Q_{org}=30$–$500$ μml/min | Flow rates of two phases, interfacial tension, contact angle | Laminar flow, plug flow, cobble flow, droplet flow |
| Salim et al. (2008) | Quartz, glass; T-junction; $d_h=793$, 667 | Water–mineral oil; $u_{aqu}=0$–$40$ cm/s, $u_{org}=0$–$20$ cm/s | Material of microchannel, hydraulic diameters, flow rates of two phases | Quartz microchannel: droplet flow, slug flow, stratified flow glass microchannel: droplet flow, semi-stratified flow, stratified flow |
| Cubaud and Mason (2008) | Glass and silicon; Cross-shaped junction | Isopropanol–PDMS oil, Ethanol–PDMS oil, PDMS oil –ethanol–glycerol 70*, PDMS oil–glycerol, PDMS oil–water–glycerol; $Q=0.1$–$200$ μ1/min | Viscosity of two phases, interfacial tension | Thread flow, jet flow, droplet flow, tube flow, displacement |
| Kashid and Kiwiminsker (2011) | T-junction with square cross section, $d_h=400$; T-junction with trapezoidal cross section, $d_h=400$; Y-junction, $d_h=269$; Concentric | Water–toluene; $u_{aqu}=0$–$1$ m/s, $u_{org}=0$–$1$ m/s | Flow rates of two phases, microchannel geometry | Slug flow, slug–drop flow, deformed interface flow, annular/parallel flow |
| Sarkar et al. (2012) | Glass; Serpentine microchannel, | Water–butanol, $Q=0$–$10$ ml/min | Flow rates of two phases | Slug flow, slug and droplet flow, droplet flow, unstable annular flow, annular flow, annular dispersed flow, fully dispersed flow |
| Fu et al. (2012) | PMMA; Flow-focusing; $h\times w=600\times600$, $400\times400$ | 0.5% SDS/water–oil; 0.5%SDS/glycerol–oil | Flow rates of two phases, interfacial tension, | Viscous displacement, tube flow, plug flow, monodispersed flow, jet flow |
| Tsaoulidis et al. (2013) | FEP, Tefzel, glass; T-junction, Y-junction; $d_h=200$, 270 | Water–IL, $Q_{total}=0.065$–$214.9$ cm$^3$/h, $Q_{IL}/Q_{total}=0.05$–$0.8$ | Material of microchannel, hydraulic diameters, ionic liquid volume fractions | Plug flow, quasi annular flow, disturbed plug, throat annular flow, plug and drop train flow, rivulet annular flow, intermittent flow, drop flow, dispersed flow, irregular flow |
| Derzsi et al. (2013) | Cross-shaped junction, cross-shaped junction with additional orifice, cross-shaped junction with an orifice and a wider outlet | Polymeric solutions–silicone oil, Polymeric solutions–PDMS oil; $Q_d=100$–$500$ μL/h, $Q_c=75$–$10{,}000$ μL/h | Elasticity of the continuous liquid, microchannel structure, flow rates of two phases | Drop without satellite, drop with a single satellite, drop with multiple satellite, jet flow |
| Fu et al. (2015) | PMMA; T-junction; $h\times w=400\times400$, $400\times600$, $400\times800$ | CMC solutions–cyclohexane; $Q_{aqu}=0$–$300$ ml/h, $Q_{org}=0$–$200$ ml/h | Microchannel dimensions, flow rates of two phases, the concentration of CMC solutions | Slug flow, droplet flow, jet flow, parallel flow |

**Table 2** (continued)

| Ref. | Microchannel features (material; structure; dimension/μm) | Continuous phase–dispersed phase system; flow condition | Parameters varied | Flow patterns |
|---|---|---|---|---|
| Plouffe et al. (2016a) | Stainless steel 316, Hastelloy C22™; SZ, TG, Venturi and Sickle | NaOH solution–n-butanol or toluene; $Q_o = Q_a = 0.40–22.15$ ml/min | Microchannel geometry, flow rates of two phases | Slug flow, drop flow, parallel flow, dispersed flow |
| Plouffe et al. (2016b) | Stainless Steel 316 Serpentine microchannel, $d_h = 700$ | NaOH solution–solution of the acetate in either n-butanol, n-hexanol, MTBE or Toluene; $Q_o = Q_a = 0.40–16$ ml/min | Properties of two phases, flow rates of two phases | Slug flow; drop flow; parallel flow |
| Darekar et al. (2017) | Glass; Y-junction; $d_h = 260, 760$ | n-butanol–water, n-butyl acetate–water, toluene–water; $Q_o = 0–10$ ml/min, $Q_a = 0–10$ ml/min | Flow rates of two phases microchannel diameters, interfacial tension, hydrophobicity | Slug flow, droplet flow, slug and droplet flow, parallel flow |
| Wu et al. (2017) | Co-flow, Flow focusing; $R_{in} = 400$, $R_{out} = 800$ | | Capillary number of continuous phase, local geometry | Droplet flow, jet flow, transition flow |
| Mahdi et al. (2017) | PTFE; T-Junction; $d_h = 250$ | Vaseline oil–water; $Q_{aqu} = 2.78 \times 10^{-11}$ $m^3/s$-$5.28 \times 10^{-9}$ $m^3/s$, $Q_{org} = 2.78 \times 10^{-10}$ $m^3/s$-$1.94 \times 10^{-9}$ $m^3/s$ | Position of the T-junction, velocities of two phases | Drop flow, plug flow, and annular flow |
| Liu et al. (2018) | PMMA; Flow-focusing; $h \times w = 400 \times 400$ | IL–water; $Q_{IL} = 0.5–120$ ml/h, $Q_{aqu} = 1.0–120$ ml/h | Flow rates of two phases | Plug flow, drop flow, jet flow, irregular flow, string of sausages |
| Cao et al. (2018) | Cross-shaped junction, $h \times w = 600 \times 600$, $400 \times 400$, $200 \times 200$, $300 \times 600$; T-junction, $h \times w = 300 \times 600$ | Water–butanol, water–toluene, water–hexane, water–oil; $Q_{aqu} = 0–60$ ml/h, $Q_{org} = 0–12$ ml/h | Flow rates of two phases, micorchannel geometry, properties of two phases | Annular flow, slug flow, slug flow with satellite, slug flow with droplet, droplet flow, droplet and slug train flow |
| Zhang et al. (2019) | PTFE; Circular; $d_h = 800, 1200, 1800$ | Toluene–$H_2SO_4$, toluene–water, ethyl acetate–water | Temperature, properties of two phases, microchannel dimensions | Droplet flow, slug flow, irregular slug flow, slug–dispersed flow, slug–annular flow, annular flow, annular–dispersed flow, droplet–dispersed flow |

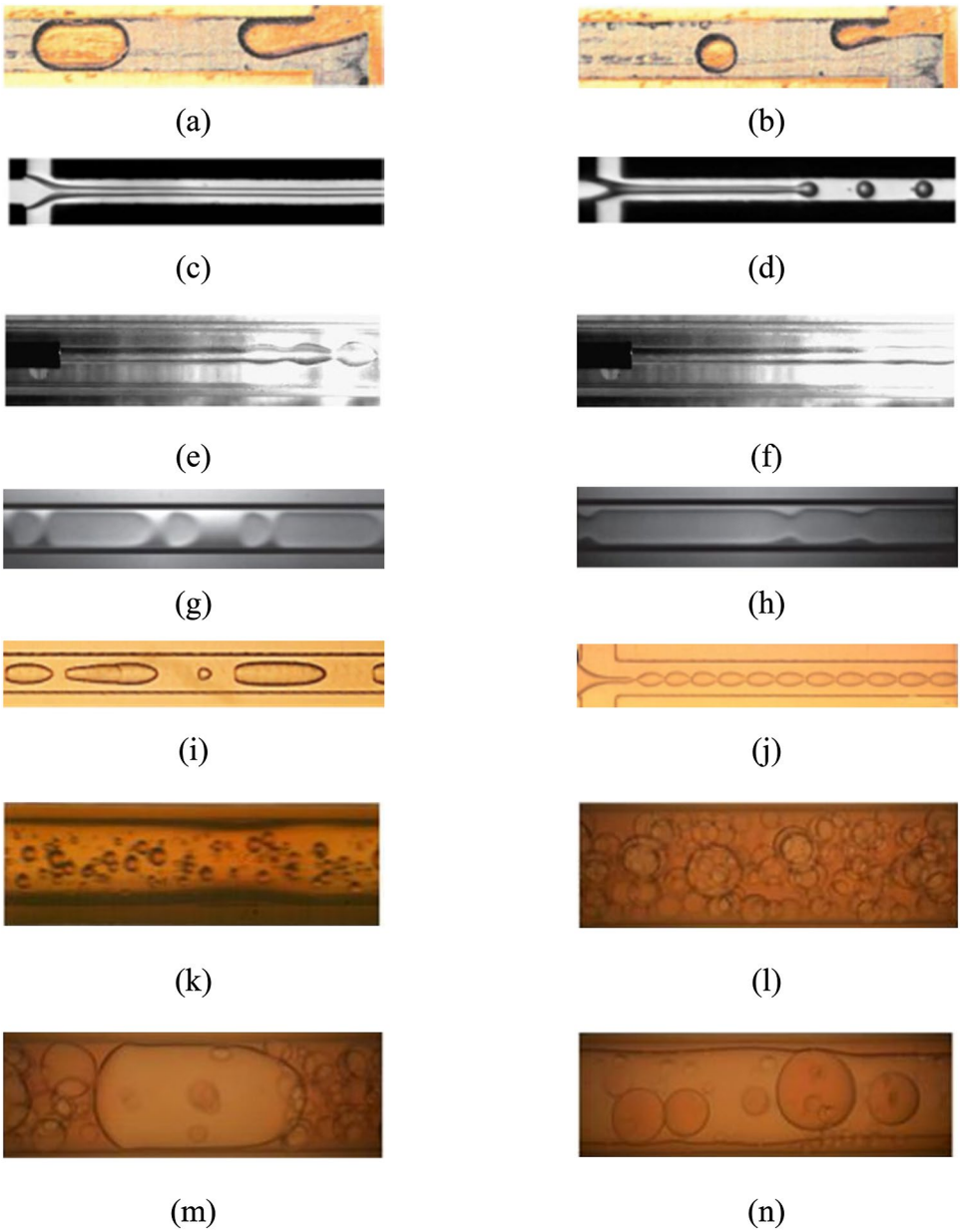


**Fig. 1** Representative flow patterns in published literature. **a** slug flow (Zhao et al. 2006); **b** droplet flow (Zhao et al. 2006); **c** thread flow (Cubaud and Mason 2008); **d** jet flow (Cubaud and Mason 2008); **e** deformed interface flow (Kashid and Kiwiminsker 2011); **f** annular/parallel flow (Kashid and Kiwiminsker 2011); **g** intermittent flow (Tsaoulidis et al. 2013); **h** throat annular flow (Tsaoulidis et al. 2013); **i** irregular flow (Liu et al. 2018); **j** string of sausages (Liu et al. 2018); **k** annular–dispersed flow (Zhang et al. 2019); **l** droplet–dispersed flow (Zhang et al. 2019); **m** slug–dispersed flow (Zhang et al. 2019); **n** annular–dispersed flow (Zhang et al. 2019)

**Table 3** Contact angles on borosilicate glass and Teflon plates by Tsaoulidis et al. (2013)

| 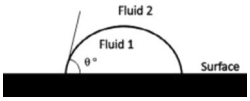  | [C4mim][NTf2]–Deionised water ($\theta°$) | [C4mim][NTf2]–Air ($\theta°$) | Deionised water–air ($\theta°$) |
|---|---|---|---|
| Borosilicate glass | 94 | 43 | 55 |
| Teflon | 70 | 64 | 102 |

contact angles on borosilicate glass and Teflon plates which were measured by Tsaoulidis et al. (2013). Results showed that the main patterns observed in glass microchannels were plug, plug and drop train and dispersed flow; while in the Teflon microchannel, annular, plug and droplet flow prevailed. More important, the authors found that in glass microchannel, the continuous phase and dispersed phase were determined by the fluid which initially filled the microchannel. With water initially saturated in a glass microchannel, it became the continuous phase. However, in a Teflon microchannel, whether the water was initially saturated or

**Table 4** Contact angle before and after surface modification by Zhao et al. (2010)

| Microchannel material | Two-phase system | Surface modification method | Contact angle before and after surface modification ($\theta^\circ$) | |
|---|---|---|---|---|
| | | | Water | Oil |
| PMMA | Water–kerosene | Coat the channel walls by alumina hydroxide sol | Before: 76<br>After: 8 | |
| Stainless steel | Water–n-butanol | Coat the channel walls by physisorption silicon sol | Before: 54<br>After: 0 | Before: 0<br>After: 17.5 |

an ionic liquid was initially saturated, the ionic liquid was always the continuous phase.

Xu et al. (2006) studied flow patterns in n-octane–water system; contact angle of oil phase was changed by adding different amount of sodium dodecyl sulfate (SDS) in water. Results showed that the contact angle increased with the addition of SDS. The contact angle increased up to more than 90° when the SDS concentration exceeded a critical micellar concentration (0.05% w/w). When the contact angle was more than 90°, ordered flow of drops can be formed. To investigate the effect of contact angle on flow patterns, Zhao et al. (2010) made surface modification on a PMMA microchannel and a stainless steel mcirochannel. The changes of contact angle before and after modification are presented in Table 4. Flow patterns before surface modification were presented as slug, monodispersed drop and parallel flow. However, after the surface modification, only parallel flow was observed.

Compared with experiments, numerical simulation provides an alternative way to study the effect of contact angle on flow patterns. Sang et al. (2009) varied the contact angle from 130° to 180°, and measured the droplet length for different contact angles. Results showed that the increase of the contact angle led to a decrease of the droplet length. This effect became lower when the contact angle was larger than 165°. Further, Raj et al. (2010) observed flow patterns for different contact angles including 60°, 90°, 120°, 140°, 160°, 180° by the VOF (volume of fluid) method. With increasing contact angle, parallel flow, slug flow and droplet flow were observed in turn. More importantly, when the contact angle was increased form 160° to 180°, the droplet length changed marginally. The same results were also presented by Bashir et al. (2011). They studied the effect of contact angle on droplet length by the level set method. Droplet lengths for various contact angles and capillary numbers were measured. Results indicated that with the contact angle greater than 165°, the droplet length remained nearly constant for all capillary numbers considered. It can be seen that when the contact angle is larger than a certain value, approximately 165°, the effect on droplet length becomes marginal.

The most common inlet structures of microchannel are T-junction, Y-junction and Cross-shaped junction. Raj et al. (2010) conducted simulations for determining the effect of inlet structure on the slug formation process. The slug size was measured in cross-shaped T-junction, T-junction and Y-junction and results indicated that the inlet structures only had minor influence on slug size. Qian et al. (2019) investigated the effect of microchannel geometry on the slug formation process. Both the dispersed phase channel width and channel depth were considered, and quantitative analyses were presented based on the dimensionless numbers. The results gave a constructive reference for determining the microchannel geometry. Dessimoz et al. (2008) carried out experiments in water–toluene systems to investigate the flow patterns in microchannel with Y-junction and T-junction. Results presented that for all volumetric flow rates used in the experiments, Y-junction always led to a parallel flow, while slug flow was formed in T-junction. Kashid and Kiwiminsker (2011) carried out experiments to identify the flow patterns in microchannels with different cross sections and contacting geometries. Four different microchannels which named T-square, T-trapezoidal, Y-rectangular and concentric as shown in Fig. 2 were used. Flow patterns including slug, slug–drop, deformed interface and parallel/annular were observed in all tested microchannels. Wu et al. (2017) developed an unsteady model of droplet formation to investigate the role of microchannel geometry on droplet formation. Axisymmetric microchannels called co-flow and flow-focusing as shown in Fig. 3 were designed and used for simulation. Drop flow, transition flow and jet flow were observed in both microchannels. Results also indicated that the co-flow microchannel had great superiority for producing monodispersed droplet, while the flow-focusing microchannel performed well in producing droplets with higher frequency. For improving the droplet formation frequency, Wang et al. (2011) made a slight modification of an ordinary T-junction microchannel—the continuous phase channel was designed with an equicrural trapezoid block to form a venturi-shaped neck—and called venturi-shaped microchannels. Results indicated that the venturi-shaped microchannels could produce smaller

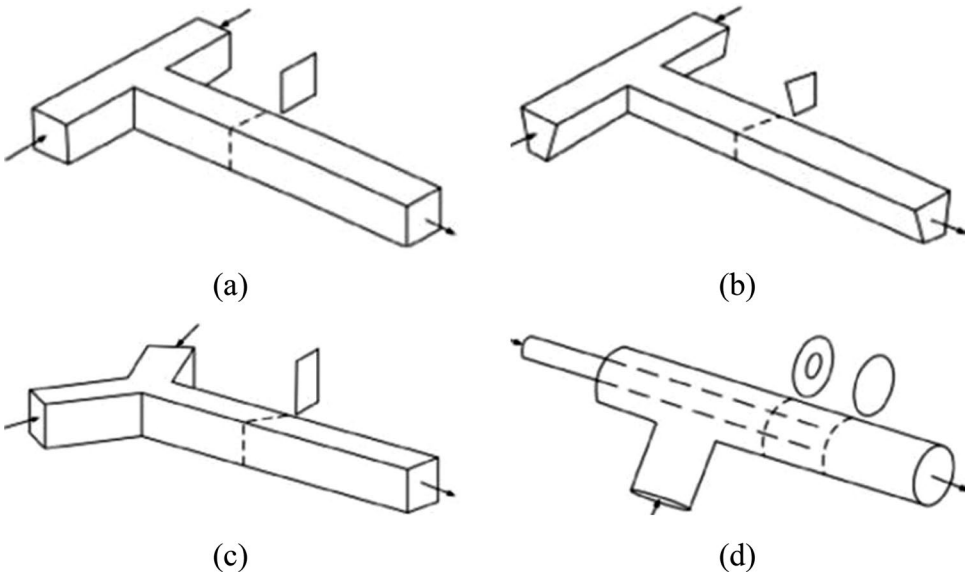


**Fig. 2** Different microchannels used by Kashid and Kiwiminsker. (2011). **a** T-square; **b** T-trapezoidal; **c** Y-rectangular; **d** concentric

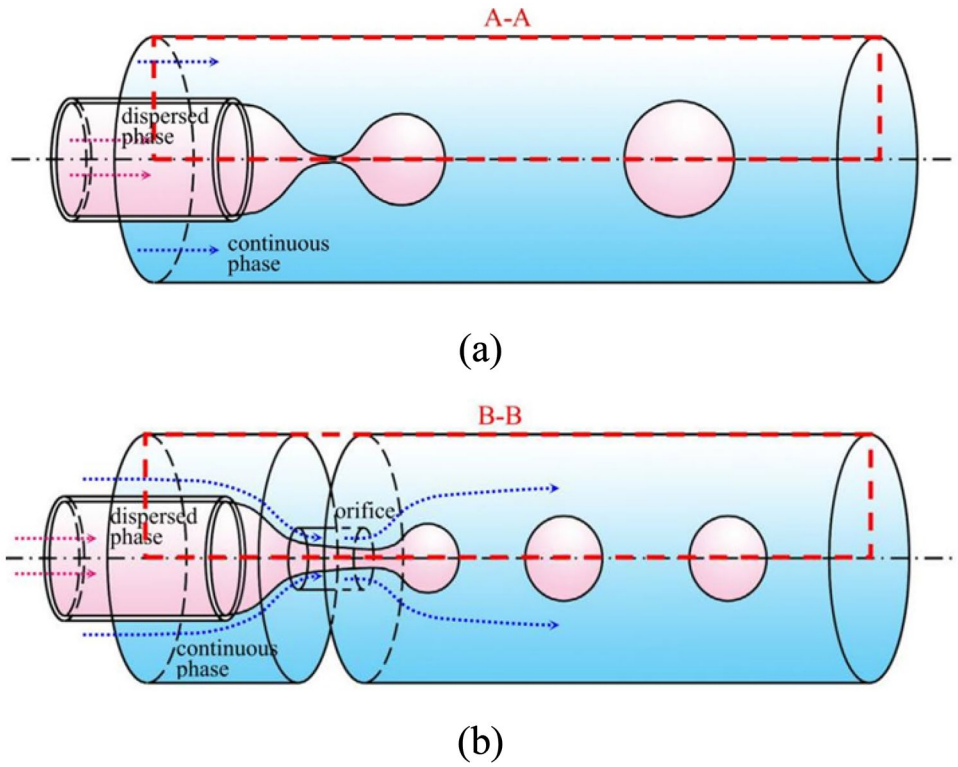


**Fig. 3** Axisymmetric microchannels used by Wu et al. (2017). **a** Co-flow; **b** flow-focusing

droplets with a higher frequency compared with T-junction microchannels at the same flow conditions. The authors further studied the effect of venturi-shaped neck position on droplet formation. Results showed that with a suitable position, the venturi-shaped microchannels could save more than 90% of the continuous phase when producing a droplet with same diameter in T-junction microchannels. Further, Derzsi et al. (2013) compared flow patterns which were observed in microchannels with three different configurations as shown in Fig. 4. In all three microchannels, the same sequence of flow pattern transitions was observed which included drop without satellites, drop with single satellite, multiple satellites and jet flow. Detailed study showed that by comparing FF-2 and FF-3, the dimension of the outlet had no influence on the droplet size in droplet flow. However, in jet flow, the FF-3 with a wider outlet could produce droplets with larger diameter. In addition, flow patterns in microchannels with more complex structures were investigated by Plouffe et al.

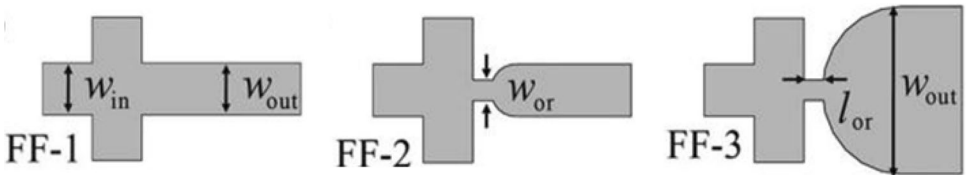


**Fig. 4** Microchannels with three different configurations used by Derzsi et al. (2013). FF-1: ordinary cross-shaped micorchannel; FF-2: cross-shaped microchannel with contraction; FF-3: cross-shaped microchannel with contraction and a wider outlet

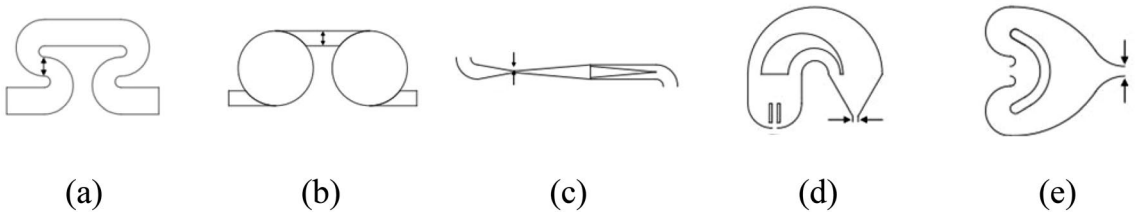


**Fig. 5** Different microchannels used by Plouffe et al. (2016). **a** SZ; **b** TG; **c** Venturi; **d** Sickle; **e** Spade

(2016). Microchannels named SZ, TG, Venturi, Sickle and Spade as shown in Fig. 5 were used in the experiments. With an increase of flow rates, slug, parallel, drop and dispersed flows were captured in sequence in microchannels of SZ, TG and Spade. In the microchannels of Venturi and Sickle, there was no parallel flow observed.

2. Effect of physical properties on flow patterns

Properties of two phases include densities of two phases, viscosities of two phases and interfacial tension. In microscale, inertia force and gravity are less important which means that the effect of density can be negligible. Many researches have been conducted to confirm the effects of viscosities of two phases and interfacial tension on flow patterns. For Newtonian system, Liu and Zhang (2009) investigated the role of viscosity ratio on flow patterns. Results showed that for a critical capillary number ($Ca_c = 0.018$), viscosity ratio may influence the drop size only when $Ca > Ca_c$ and the drop size is decreased with an increase of viscosity ratio. Gupta and Kumar (2010) analyzed the continuous phase viscosity on flow patterns. Results showed that at large flow rate ratio ($\Phi = 1/5$), an increase of the continuous phase viscosity made the flow patterns to transform from parallel flow to droplet flow. Higher continuous phase viscosity was more beneficial for droplet flow. Feigl et al. (2014) investigated the effect of the continuous phase viscosity and dispersed phase viscosity on flow patterns, respectively. The constant viscosity ratio of $\lambda = 6$ was achieved by increasing the dispersed phase viscosity or decreasing the continuous phase viscosity. The dispersed phase velocity was kept as 0.011 m/s in both cases. It was shown that when increasing the dispersed phase viscosity, the flow patterns changed from droplet flow to jet flow. To maintain the droplet flow, the dispersed phase velocity should be decreased to 0.0011 m/s. However, when decreasing the continuous phase viscosity, the droplet flow was prevailed. Wehking et al. (2014) also investigated the effect of viscosity ratio on flow patterns. The flow pattern transition from droplet flow to parallel flow was easily happened at low viscosity ratio.

Viscosity of Newtonian fluids and non-Newtonian fluids has different effects on flow patterns. Sang et al. (2009) investigated the effects of continuous phase viscosity on drop size. Both Newtonian and non-Newtonian fluids were considered. Results indicated that the increase of viscosity in Newtonian fluids and power-law fluids reduced the drop size. However, in Bingham fluids, the increase of viscosity had less effect on drop size. The 960% variation of viscosity only made a 4% variation of drop size. Experiments were carried out by Derzsi et al. (2013) to illustrate the dynamics of Newtonian droplet formation in non-Newtonian/Newtonian systems. Comparatively, Newtonian droplet formation in Newtonian/Newtonian systems was presented as well. In Newtonian/Newtonian systems, the continuous phase of Newtonian fluid shared the same shear viscosity with the non-Newtonian counterpart. Figure 6 displays the comparisons of flow pattern in Newtonian/Newtonian (N) and non-Newtonian/Newtonian (nN) systems.

In Fig. 6, the columns and rows illustrated the drop formation in various flow rate ratios and the dispersed phase viscosities. It can be seen that the droplet shape was more deformed when the continuous phase is the non-Newtonian fluid. It can be seen that the droplet in Newtonian/Newtonian system was nearly spherical and the shapes kept constant when the droplet moved downstream. While in

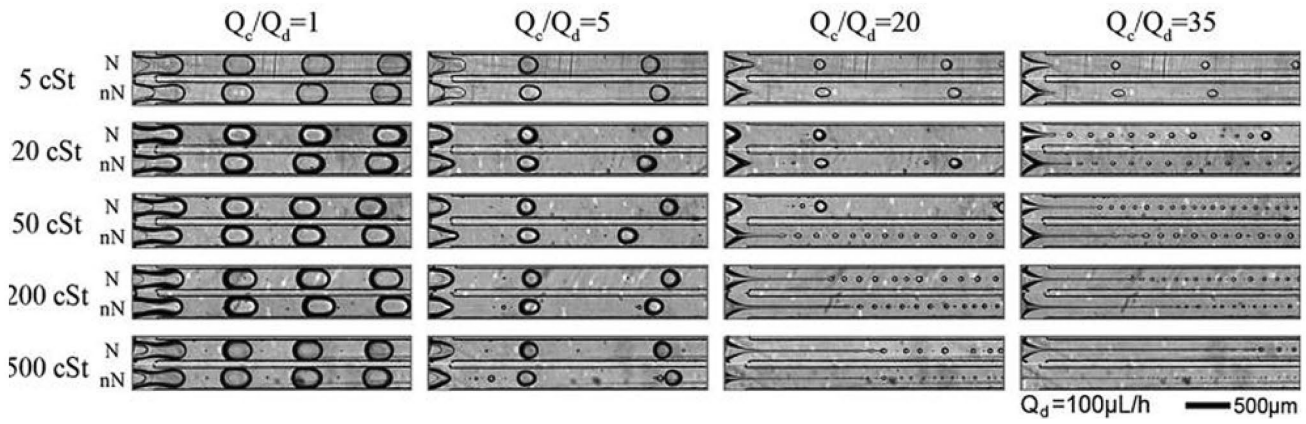


**Fig. 6** Examples of flow patterns in Newtonian/Newtonian (N) and non-Newtonian/Newtonian (nN). systems observed by Derzsi et al. (2013)

non-Newtonian/Newtonian system, the droplet transformed from elliptical shapes to bulleted shapes. The deformation rate of droplet was increased with an increase of the continuous phase flow rate. In addition, elasticity of the non-Newtonian fluid made a more stable jet flow compared with the Newtonian fluid. Other remarkable results indicated that viscoelastic liquids had superiority to produce droplet with higher frequency at low flow rates. Fu et al. (2015) conducted experiments to investigate the flow patterns of Newtonian (dispersed phase)/non-Newtonian fluids (continuous phase) two-phase flow. Four flow patterns were mainly observed which included slug flow, drop flow, jet flow and parallel flow. The non-Newtonian fluids were carboxyl methyl cellulose (CMC) in demineralized water with different concentrations. The increases of concentration of CMC led to an increase of viscosity. Thus, it was made possible to form droplet flow even at a low dispersed phase velocity. Liu et al. (2018) investigated dynamics of water–ionic liquid ([BMIM] [PF6]) two-phase flow in a flow-focusing microchannel. The ionic liquid had a high viscosity of 251.76 mPa s. By changing the flow rates of the two phases, flow patterns which included dripping, jetting, irregular and string of sausages were observed. In addition, the droplet formation mechanisms in Newtonian and non-Newtonian fluids were also compared with Cubaud and Mason (2008), Qiu et al. (2010) and Chiarello et al. (2015).

Interfacial tension is related to properties of two phases. Dessimoz et al. (2008) studied effect of interfacial tension on flow patterns in water–toluene system. Solutes were added in water and toluene for changing the interfacial tension of the systems. Results showed that at lower interfacial tension, flow patterns were parallel flow dominated. With an increase of interfacial tension, slug flow was observed. Timung et al. (2015) studied the effect of viscosity and interfacial tension on flow patterns. With reduction of interfacial tension, flow patterns including slug, plug, drop, core-annular and stratified were presented in sequence. Darekar et al. (2017) investigated the effect of interfacial tension on flow patterns. The variation of interfacial tension was achieved using different two-phase systems which included water/n-butanol, water/n-butyl acetate and water/toluene. The interfacial tension was 1.75 mN/m, 14.1 mN/m and 36 mN/m, respectively. Results showed that in water/toluene system with the highest interfacial tension, slug flow was dominating among all flow patterns. With the decrease of interfacial tension, parallel flow was more pronounced. Wehking et al. (2014) investigated the effect of interfacial tension on flow patterns and the transition lines of droplet flow to parallel flow were compared. Raj et al. (2010) also investigated the effect of viscosity and interfacial tension on slug size.

## 3. Effect of flow rate on flow patterns

Flow rate is an important parameter affecting the flow patterns. It can be easily changed to achieve various flow patterns. Generally, slug flow is more observed at a low flow rate of both phases. When the continuous phase flow rate increases while the dispersed phase flow rate is kept constant, droplet flow is presented. In contrast, when the dispersed phase flow rate increases while the continuous phase flow rate is kept constant, parallel flow is emerged (Kashid and Kiwiminsker 2011; Darekar et al. 2017).

Up to now, nearly all researches have been operated at room temperature. However, in actual conditions, temperature is also a non-negligible factor on liquid–liquid two-phase flow patterns. Zhang et al. (2019) conducted experiments at different temperatures to investigate the effect of temperature on liquid–liquid two-phase flow hydrodynamics. Three temperatures, namely 0.5, 10 and 25 °C, were selected for experiments. Physical properties of each fluid were measured at different temperatures as shown in Table 5. The viscosities of water and 92% $H_2SO_4$ presented highly

**Table 5** Physical properties of the fluids at different temperatures by Zhang et al. (2019)

| $T/°C$ | Toluene | Ethyl acetate | | Water | | 92% $H_2SO_4$ | |
|---|---|---|---|---|---|---|---|
| | μ/m Pa·s | μ/m Pa·s | $\sigma_{e\text{-}w}$/m N/m | μ/m Pa·s | $\sigma_{t\text{-}w}$/m N/m | μ/m Pa·s | $\sigma_{t\text{-}h}$/m N/m |
| 0.5 | 0.76 | 0.56 | 8.29 | 1.76 | 34.5 | 45.8 | 13.67 |
| 10 | 0.67 | 0.50 | 7.62 | 1.31 | 34.92 | 30 | 14.81 |
| 25 | 0.55 | 0.42 | 7.23 | 0.89 | 35.48 | 18 | 13.77 |

sensitivity to temperature. In all experiments, the oil phase was the continuous one, while the aqueous phase was the dispersed one. Thus, an increase of temperature directly led to a decrease of dispersed phase viscosity. According to the authors, the dispersed phase viscosity played an important role in the flow pattern transition from slug to annular flow. Thus, the increase of temperature made the slug flow to dominate the flow pattern map.

### 2.2.2 Flow pattern maps

Flow pattern maps are plotted for identifying the flow pattern transitions distinctly. Parameters such as velocity of two phases (Salim et al. 2008; Kashid and Kiwiminsker 2011; Fu et al. 2015; Mahdi et al. 2017; Cao et al. 2018), flow rates of two phases (Zhao et al. 2006; Sarkar et al. 2012; Darekar et al. 2017; Mahdi et al. 2017), Capillary numbers (Cubaud and Mason 2008; Darekar et al. 2017), Weber numbers (Fu et al. 2012; Darekar et al. 2017) and so on (Wu et al. 2017; Zhang et al. 2019) are mainly used as coordinates for plotting flow pattern maps.

Zhao et al. (2006) plotted flow pattern maps as shown in Fig. 7(a) based on Weber number of two phases. The flow pattern maps were divided into three regions and corresponding criteria were proposed as:

I: the interfacial tension-dominated region, including slug flow, monodispersed flow parallel flow with smooth interface, for $(We_{KS}<1)\cap(We_{WS}<1)$; II: region where the inertia and interfacial tension were comparable, including parallel flow with wavy interface and droplet populations, for $[(We_{KS}<10)\cap(We_{WS}<10)]\cap[(We_{WS}>1)\cup(We_{KS}>1)]$; III: the inertia-dominated region, including droplet populations and chaotic thin striations flow, for $(We_{KS}>10)\cup(We_{WS}>10)$.

Kashid and Kiwiminsker (2011) observed flow patterns in different microchannel structures and flow pattern maps were plotted based on velocities of the two phases as shown in Fig. 7b–d. By comparing the three flow pattern maps, flow pattern transitions with increasing velocity of the two phases could be distinguished obviously. Furthermore, a criterion for identifying flow patterns in a given microchannel was proposed as: surface tension-dominated region: $Re_d d_h/\varepsilon_d<0.1$ m; Transition region: $0.1\ \text{m}<Re_d d_h/\varepsilon_d<0.35$ m; Inertia-dominated region: $Re_d d_h/\varepsilon_d>0.35$ m.

Wehking et al. (2014) carried out nearly one hundred experiments for identifying hydrodynamics of liquid–liquid two-phase flow. Critical capillary numbers were proposed to predict flow pattern transitions from droplet to parallel.

$$Ca=c_0\Gamma^{c_1}\Omega^{c_2}\lambda^{c_3}\Phi^{c_4}, \tag{1}$$

where $c_0\sim c_4$ are constants and have different values in slug/parallel transition and drop/parallel transition. $\Omega$ represents the dimensionless interfacial tension.

Fu et al. (2015) investigated flow patterns of non-Newtonian systems and plotted the flow pattern maps based on velocity of the two phases as shown in Fig. 7e. Based on Weber number, microchannel dimension and viscosity of the two phases, a general model was proposed for predicting flow pattern transitions including slug/drop transition line, drop/jet transition line, slug/jet transition line and parallel/jet transition line.

$$c_0We_c^{c_1}(h/w)^{c_2}\delta^{c_3}(\mu_c/\mu_d)^{c_4}=We_d^{c_5}(h/w)^{c_6}\delta^{c_7}(\mu_c/\mu_d)^{c_8}, \tag{2}$$

where $c_0\sim c_8$ are constants and have different values for each transition. $\delta$ represents the dimensionless surface roughness. The viscosity of non-Newtonian fluid was calculated based on Carreau model. The experimental conditions were: $2.185\times10^{-3}<Ca_c<9.27\times10^{-2}$, $3.643\times10^{-3}<Re_c<17.1528$, $7.9605\times10^{-6}<We_c<0.9770$, $5.5181\times10^{-6}<Ca_d<4.258\times10^{-3}$, $9.63\times10^{-3}<Re_d<80.2537$, $5.3142\times10^{-7}<We_d<0.3417$.

Cao et al. (2018) also plotted flow pattern maps based on velocity of the two phases as shown in Fig. 7f. A general empirical correlation was proposed for identifying flow pattern transitions including annular/slug transition and slug/drop transition.

$$c_0Re_c^{c_1}We_c^{c_2}=Re_d^{c_3}We_d^{c_4}, \tag{3}$$

where $c_0\sim c_4$ are constants and have different values for each transition.

Zhang et al. (2019) carried out comprehensive experiments to study effects of temperature, properties of fluids and microchannel dimensions on flow patterns. Figure 7g and h present the flow pattern maps in different two-phase systems based on capillary number of the continuous phase and Reynolds number of the dispersed phase. Flow patterns which include droplet flow, slug flow, irregular slug

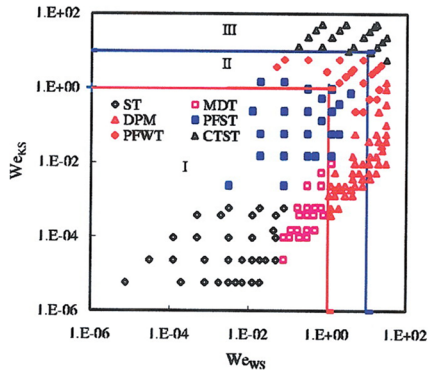
1.E+02
1.E+00
1.E-02
1.E-04
1.E-06
We_KS
We_WS
III
II
I
ST
DPM
PFWT
MDT
PFST
CTST

(a)

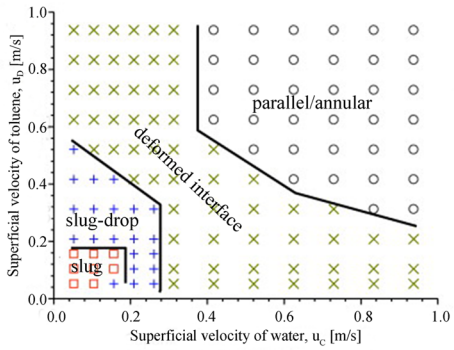
Superficial velocity of toluene, u_D [m/s]
Superficial velocity of water, u_C [m/s]
parallel/annular
deformed interface
slug-drop
slug

(b)

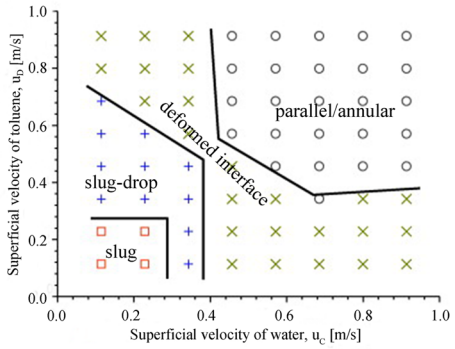
Superficial velocity of toluene, u_D [m/s]
Superficial velocity of water, u_C [m/s]
deformed interface
parallel/annular
slug-drop
slug

(c)

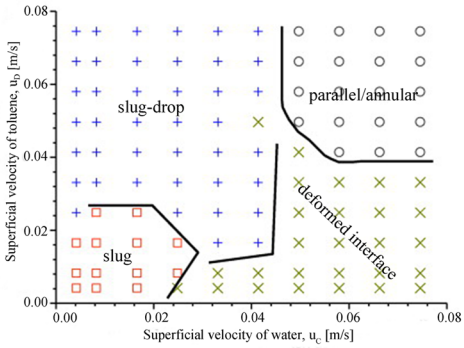
Superficial velocity of toluene, u_D [m/s]
Superficial velocity of water, u_C [m/s]
slug-drop
parallel/annular
slug
deformed interface

(d)

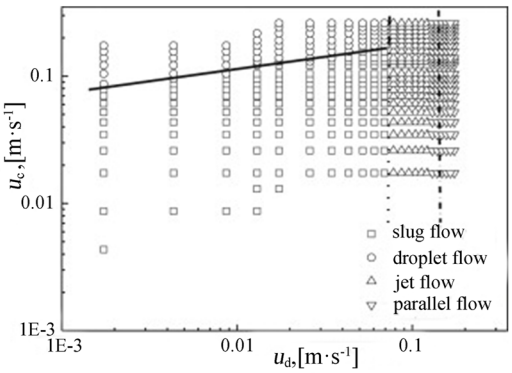
u_c, [m·s^-1]
u_d, [m·s^-1]
slug flow
droplet flow
jet flow
parallel flow

(e)

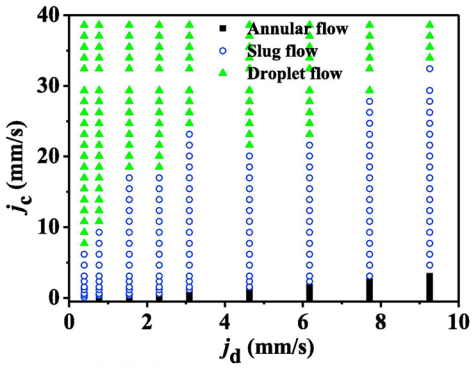
j_c (mm/s)
j_d (mm/s)
Annular flow
Slug flow
Droplet flow

(f)

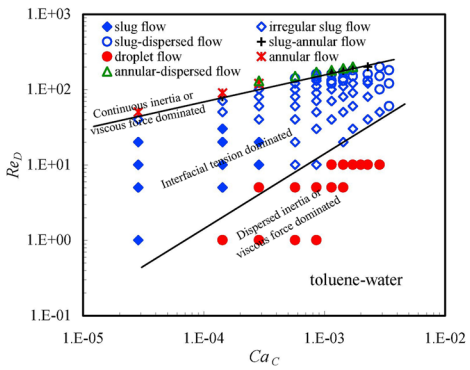
Re_D
Ca_C
slug flow
slug-dispersed flow
droplet flow
annular-dispersed flow
irregular slug flow
slug-annular flow
annular flow
Continuous inertia or viscous force dominated
Interfacial tension dominated
Dispersed inertia or viscous force dominated
toluene-water

(g)

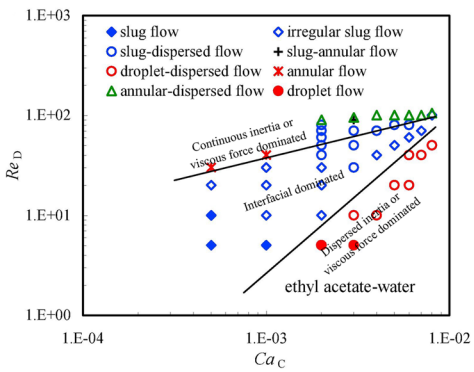
Re_D
Ca_C
slug flow
slug-dispersed flow
droplet-dispersed flow
annular-dispersed flow
irregular slug flow
slug-annular flow
annular flow
droplet flow
Continuous inertia or viscous force dominated
Interfacial dominated
Dispersed inertia or viscous force dominated
ethyl acetate-water

(h)

◂**Fig. 7** Typical flow pattern maps reported in literature. **a** Flow pattern maps and transition lines plotted by Zhao et al. (2006) **b** Flow pattern maps in T-square and T-trapezoidal microchannels plotted by Kashid and Kiwiminsker (2011) **c** Flow pattern maps in Y-rectangular microchannel plotted by Kashid and Kiwiminsker (2011) **d** Flow pattern maps in concentric microchannel plotted by Kashid and Kiwiminsker (2011) **e** Flow pattern maps and transition lines for flow patterns plotted by Fu et al. (2015) **f** Flow pattern maps plotted by Cao et al. (2018) **g** Flow pattern maps in toluene/water system plotted by Zhang et al. (2019) **h** Flow pattern maps in ethyl acetate/water system plotted by Zhang et al. (Zhang et al. 2019)

flow, slug–dispersed flow, slug–annular flow, annular flow, annular–dispersed flow and droplet–dispersed flow were observed. These flow patterns were divided into three regions according to the forces involved as shown in Fig. 7g and h. A general correlation was proposed as Eq. (4), to predict the slug/parallel transition and slug/drop transition.

$$Ca_{\mathrm{d}}^{0.7} Re_{\mathrm{d}}^{0.5} = \mathrm{c}_1 (Ca_{\mathrm{c}} Re_{\mathrm{c}}^{0.5})^{\mathrm{c}_2}, \tag{4}$$

where $c_1$ and $c_2$ are constants and have different values for each transition. The authors verified the universality of the proposed correlation by comparing experimental results in published literature which involved a large viscosity range from 0.85 to 1200 mPa s.

## 3 Mass transfer in liquid–liquid two-phase flow in microchannels

The overall volumetric mass transfer coefficient calculated in microchannels was more than two or three orders of magnitude higher than those in conventional reactors and the energy consumption in microchannels was far less than in conventional reactors (Zhao et al. 2007; Kashid and Agar 2007). Due to the great superiority of liquid–liquid two-phase flow in microchannels, many researches have been carried out for studying mass transfer in liquid–liquid two-phase flow in microchannels. Table 6 gives a detailed summary of volumetric mass transfer coefficients in liquid–liquid two-phase flow in microchannels tested so far.

### 3.1 Enhancement of mass transfer performance

Among all the flow patterns mentioned in Sect. 2, droplet flow and slug flow present great superiority in mass transfer performance due to the existing inner circulation in the droplet/slug and the large specific interfacial area. These two aspects are illustrated in this part in detail. In the following descriptions, the droplet is used to represent both droplet and slug.

#### 3.1.1 Inner circulation in droplets

When the droplet moves along the microchannel, due to the shear stress exerted by the wall, radial velocity gradient exists when fluids are flowing through the microchannel. The velocity reduces from the axial direction of the microchannel to the walls. However, when droplet is moving through the microchannel, not only a velocity gradient exists in the radial direction due to the shear stress exerted by the wall, but also a velocity gradients exist both in the radial direction and the axial direction. The former is induced by the interaction with the wall and the latter is caused due to the interaction with the continuous phase. Therefore, inner circulations are induced due to the velocity gradient. The inner circulation promotes the surface renewal and reduces the thickness of the boundary layer at the phase interface, so the mass transfer performance is enhanced accordingly. One of the earliest experiments for elaborating mass transfer performance enhanced by inner circulation in droplet was performed by Burns and Ramshaw (2001). Later, experiments and simulations were carried out by Kashid (2005), Kashid et al. (2007, 2008) and Kinoshita et al. (2007) to further clarify the inner circulation in the droplet and the stagnant region where the liquid velocity is zero in droplet. Particle image velocimetry (PIV) and CFD particle tracing algorithm were used for visualizing the inner circulation in a droplet.

Figure 8 presents the schematic representation of inner circulation and velocity distribution in droplets (Li and Angeli 2017). It can be seen from Fig. 8a that three pairs of inner circulation existed in the droplet. The main circulation is induced by the interaction with the wall which marked as 1. The minor circulation is induced by the interaction with the continuous phase which marked as 2.

#### 3.1.2 Specific interfacial area

The droplet flow pattern provides a uniform interfacial area which significantly promote the mass transfer process. Moreover, the uniform interfacial area makes the prediction of the overall volumetric mass transfer coefficient possible. In liquid–liquid droplet flow, the specific interfacial area is defined as the ratio of droplet surface to unit cell volume. Methods for determining the specific interfacial area can be classified into physical method and chemical method (Ghaini et al. 2010). For physical measurement, the most common method is light induced fluorescence combined with photography. By taking high-resolution images, the droplet surface area and droplet unit volume can be calculated and the specific interfacial area is obtained as well. However, the main difficulties lie in the simplification of the droplet shape and the measurement of the film thickness. Figure 9 shows the schematic diagram of droplet flow in microchannels with and without film. In Fig. 9, $L_{\mathrm{d}}$, $L_{\mathrm{U}}$, $R$, $w$ and $h$ represent the

**Table 6** A summary of overall volumetric mass transfer coefficients in liquid–liquid two-phase flow in microchannels in published literature

| Ref. | Features of microchannel (material, inlet structure and dimension/μm) | Two-phase systems and flow conditions | Flow patterns | $k_La/s^{-1}$ |
|---|---|---|---|---|
| Plouffe et al. (2016a) | Stainless steel 316, Hastelloy C22™; SZ, TG, Venturi, Sickle and spade | Aqueous phase: water + NaOH ($C_{NaOH,aqu}$ = 0.5 M), Organic phase: n-butanol/toluene + acetate ($C_{acetate,org}$ = 0.05 M); $Q_{aqu} = Q_{org}$ = 0.4–22.15 ml/min | Slug flow, droplet flow, parallel flow, dispersed flow | Water/n-butanol: SZ: 0.535–0.813, TG: 0.432-0.821, Venturi: 0.633–0.845, Sickle: 0.688–0.843,Spade: 0.569–0.825<br>Water/toluene: SZ: 0.170–0.431,TG: 0.168–0.466, Venturi: 0.244–0.487, Sickle: 0.231–0.493, Spade: 0.147–0.326: |
| Zhao et al. (2010) | PMMA, stainless steel; Opposed T-junction, $w_c \times w_d \times h = 600 \times 600 \times 300$ | Aqueous phase: Water, Organic phase: n-butanol + succinic acid; $Re$ = 11–275 | Parallel flow, slug flow, monodispersed flow | Before surface modification: 0.27–8.93, after surface modification: 0.19–11.96 |
| Qian et al. (2019) | Glass; Y-junction: $d_h$ = 269; T-junction: $d_h$ = 400 | Aqueous phase: water + NaOH ($C_{NaOH,aqu}$ = 0.15–0.3 M); Organic phase: toluene/hexane + $CCl_3COOH$ ($C_{CCl3COOH,org}$ = 0.6 M); $u_{total}$ = 3–46 mm/s, $\Phi$ = 1 | Parallel flow, slug flow | 0.2–0.5 |
| Zhao et al. (2007) | Stainless steel; T-junction; $w \times h$=600 × 300, 600 × 600; $w \times h$=600 × 300: $u_{total}$ = 0.01–2.5 m/s; $w \times h$=600 × 600: $u_{total}$ = 0.005–2 m/s; $Re_M$ = 19–650 | Aqueous phase: water, Organic phase: n-butanol + succinic acid; | Parallel flow with smooth interface, parallel flow with wavy interface, chaotic thin striations flow | 0.067–17.35 |
| Fries et al. (2008) | PDMS<br>Y-junction<br>$w \times h$ = 200 × 100, 300 × 140, 400 × 140; T-junction<br>$w \times h$ = 200 × 100: 10.8,<br>$w \times h$ = 00 × 140:1.9,<br>$w \times h$ = 400 × 140:1.1, $w$ = 100 | Aqueous phase: water + Vanillin ($C_{Vanillin,aqu}$ = 1 g), Organic phase: toluene; $Q$ = 10–150 μl/min | Y-junction: parallel flow, T-junction: slug flow | Maximum value Parallel flow: Slug flow: 5.3 |
| Ghaini et al. (2010) | PTFE; Y-junction; $d_h$ = 500, 750, 1000 | Aqueous phase: water + NaOH ($C_{NaOH,aqu}$ = 0–0.4 M)<br>Organic phase: n-Butyl formate; $Q_{aqu} = Q_{org}$ = 20–80 ml/h | Slug flow | $d_h$ = 500: 0.9–1.67, $d_h$ = 750: 0.91–1.46, $d_h$ = 1000: 0.88–1.29 |
| Xu et al. (2013) | PTFE; T-junction; $d_h$ = 600, 800, 1000 | Aqueous phase: water + NaOH ($C_{NaOH,aqu}$ = 0.2–0.4 M), Organic phase: kerosene + n-butyl acetate; $Q$ = 5–100 ml/h | Slug flow | $C_{NaOH,aqu}$ = 0.2 M, $d_h$ = 600: 0.035-0.215, $d_h$ = 800: 0.006–0.07;<br>$C_{NaOH,aqu}$ = 0.4 M, $d_h$ = 600: 0.098–0.324, $d_h$ = 800: 0.07–0.218 |
| Raimondi et al. (2014) | Silicon combined with glass; T-junction; $w \times h$ = 210 × 210, 300 × 300 | Aqueous phase: water, Organic phase: toluene + acetone; $Q_{total}$ = 5–50 ml/h | Slug flow | 0.72–8.44 |

**Table 6** (continued)

| Ref. | Features of microchannel (material, inlet structure and dimension/μm) | Two-phase systems and flow conditions | Flow patterns | $k_La/s^{-1}$ |
|---|---|---|---|---|
| Woitalka et al. (2014) | Nitride; Spiral microchannel; $d_h = 427$ | Aqueous phase: water, Organic phase: 1-butanol + succinic acid; $Q = 0.16$–6.5 ml/min; $Re = 5.3$–201 | Stratified flow, dispersed flow | 0.28–8.83 |
| | Teflon; Spiral microchannel; $d_h = 500$ | $Q = 0.16$-6.5 ml/min; $Re = 5.3$–201 | Stratified flow, dispersed flow | 0.15–3.33 |
| | Corning LFR; $d_h = 400$ | $Q = 0.45$–10.3 ml/min; $Re = 17.2$–393 | stratified flow, dispersed flow | 0.07–3.65 |
| | Corning AFR; $d_h = 1100$ | $Q = 8.7$–200.0 ml/min; Re = 146–3357 | stratified flow, dispersed flow | 0.07–3.31 |
| Zhao et al. (2012) | Glass; Cross-shaped junction; $d_h = 200$, 400, 600 | Aqueous phase: water + NaOH ($C_{NaOH,aqu} = 0.1$ M);Organic phase: n-hexane + $CH_3COOH$ ($C_{CCl3COOH,org} = 0.5$ M); $u_{total} = 10$–45 mm/s, $\Phi = 0.5$, 1, 2 | Slug flow | $\Phi = 1$; $w = 200$: 0.11–0.24,$w = 400$: 0.064–0.099, $w = 600$: 0.032–0.045 |
| Sattari-Najafabadi et al. (2017a) | Glass; Cross-shaped junction, cross-shaped T-junction, T-junction; $w \times h = 400 \times 400$, $600 \times 300$ | Aqueous phase: water + NaOH ($C_{NaOH,aqu} = 0.1$ M), Organic phase: n-hexane + $CH_3COOH$ ($C_{CCl3COOH,org} = 0.5$ M); $Q_{total} = 5$–35 ml/h, $\Phi = 0.5$, 1, 2 | Slug flow | $w \times h = 400 \times 400$: $\Phi = 0.5$: 0.070–0.111, $\Phi = 1$: 0.059–0.084, $\Phi = 2$:0.034-0.061, $w \times h = 600 \times 300$: $\Phi = 0.5$: 0.063–0.089, $\Phi = 1$:0.043–0.070, $\Phi = 2$:0.028–0.051, $w \times h = 400 \times 400$, $\Phi = 1$:Cross-shaped junction: 0.058–0.084, cross-shaped T-junction:0.049–0.078, T-junction: 0.044–0.074 |
| Kashid et al. (2011a) | T-junction with square cross section: $d_h = 400$; T-junction with trapezoidal cross section: $d_h = 400$; Y-junction: $d_h = 269$; concentric, caterpillar, $d_h = 150$ | Aqueous phase: water + acetone ($C_{acetone,aqu} = 0.6$ M), Organic phase: toluene; $Q_{org} = 1$–18 ml/min, $Q_{aqu} = 1$–18 ml/min | Slug flow, slug-drop flow, deformed interface flow, annular/parallel flow | T-junction with square cross section:0.13–1.26,T-junction with trapezoidal cross section :0.16–1.03, Y-junction:0.069–0.75,concentric:0.012–0.19, caterpillar:0.13–2.27 |

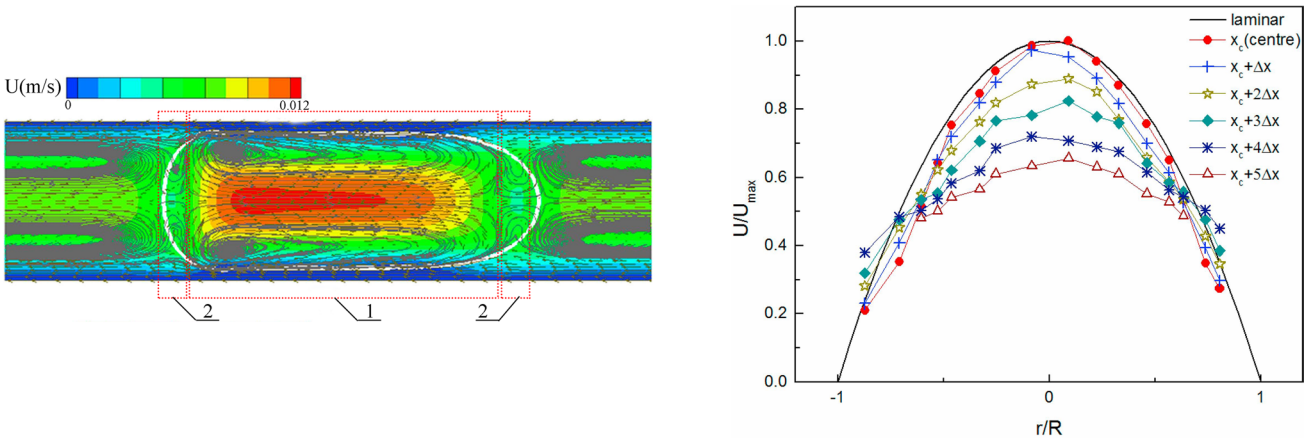


(a) Velocity distribution and inner circulation in a droplet

(b) Non-dimensional horizontal component of total velocity at different locations along a droplet

**Fig. 8** Velocity distribution and inner circulation in a droplet (Li and Angeli 2017). **a** Velocity distribution and inner circulation in a droplet. **b** Non-dimensional horizontal component of total velocity at different locations along a droplet

**Fig. 9** Schematic diagram of droplet flow in microchannels. **a** without film. **b** with film

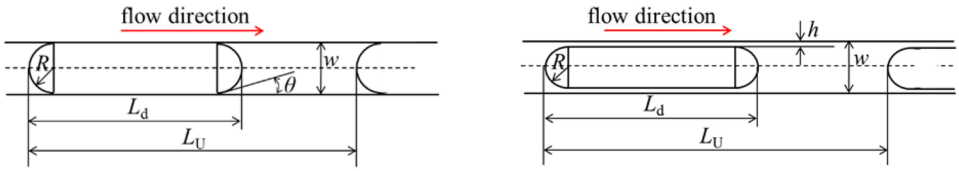


(a) without film

(b) with film

droplet length, droplet unit length, radius of droplet cap, microchannel width and film thickness, respectively.

Generally, for a droplet with regular shape as shown in Fig. 9, the droplet can be considered as a cubic combined with hemispheric shape (Raimondi et al. 2014; Sattari-Najafabadi et al. 2017a). The most used method for the prediction of the film thickness is proposed by Brethertons (Kashid and Agar 2007; Ghaini et al. 2010; Xu et al. 2013). The Brethertons law (Bretherton 1961) considers the capillary number as the significant factor for determining the film thickness. In addition, correlations for calculating the film thickness based on other parameters such as Weber number, Reynolds number or the combinations (Tsaoulidis and Angeli 2016; Dore et al. 2012) are proposed and theses correlations are summarized by Li and Angeli (2017) in detail.

### 3.2 Methods of mass transfer performance studies

Table 7 summarizes the general methods used for conducting mass transfer performance studies in liquid–liquid two-phase flow in microchannels. Experiments and simulations are included.

When conducting experiments involving reactions, neutralization of an acid with alkali is widely used in studying the mass transfer efficiency. Alkali and acid are added into the aqueous phase and organic phase, respectively. With droplets moving, the acid is transferred from the organic phase into the aqueous phase and reaction happens (Dessimoz et al. 2008; Kashid 2005; Sattari-Najafabadi et al. 2017b). One important thing is that the transferred acid should be reacted with the alkali instantaneously in order to avoid the accumulation of the acid in the organic phase and further eliminate the effect of reactions on the mass transfer performance. Indicators such as bromothymol-blue, phenol red and Sudan III are added in the aqueous phase or organic phase. The reaction process is visualized by color change of the phases including indicators. Figure 10a shows the neutralization of $CH_3COOH$ with NaOH recorded by Dessimoz et al. (2008). The color change of the aqueous phase from blue to yellow was clearly observed as droplet was moving along the microchannel. In addition, saponification and alkaline hydrolysis are also used for analyzing mass transfer efficiency (Zhang et al. 2019). The concentration of alkali in the aqueous phase was subsequently measured by

**Table 7** Experiments and simulations carried out for mass transfer performance studies in liquid–liquid two-phase flow in microchannels

| Ref. | Method | System and reaction |
|---|---|---|
| Dessimoz et al. (2008) | Experiment; Neutralization | Aqueous phase: Water + NaOH ($C_{NaOH,\ aqu}$ = 0.1–0.3 M), Organic phase: toluene or hexane + $CH_3COOH$ ($C_{CCl3COOH,\ org}$ = 0.6 M); Brom-thymol-blue was added to the aqueous phase or Sudan III was added to the organic phase as indicators; $NaOH + CH_3COOH \rightarrow CH_3COONa + H_2O$ |
| Kashid (2005) and Sattari-Najafabadi et al. (2017b) | Experiment; Neutralization of $CH_3COOH$ with NaOH; Residence time required for color change was calculated | Aqueous phase: water + NaOH ($C_{NaOH,\ aqu}$ = 0.1 M); Organic phase: n-hexane + $CH_3COOH$ ($C_{CCl3COOH,\ org}$ = 0.5 M); $NaOH + CH_3COOH \rightarrow CH_3COONa + H_2O$<br>Minute amount of phenol red was added in aqueous phase as an indicator<br>During the droplet formation process, acetic acid transfered from the n-hexane to water and reacted with sodium hydroxide. The color of aqueous phase was changed from red to yellow with the neutralization went on |
| Ghaini et al. (2010) | Experiment; Saponification; Concentration of the NaOH in outlet was measured by acid–base titration with HCl | Aqueous phase: water + NaOH, Organic phase: HCOO(CH2)3CH3; HCOO(CH2)3CH3 + OH–→HCOO–+C3H7CH2OH; Minute amount of brom-thymol-blue was added in aqueous phase as an indicator; During the droplet formation process, n-butyl formate transferred from the organic phase to aqueous phase and reacted with sodium hydroxide. The color of aqueous phase was changed from blue to green with the saponification went on |
| Xu et al. (2013) | Experiment; Alkaline hydrolysis; Aqueous phase in outlet was separated and concentration of NaOH was measured by acid–base titration | Aqueous phase: Water + NaOH ($C_{NaOH,\ aqu}$ = 0.2-0.4 M), Organic phase: saturated with n-butyl acetate; $CH_3COO(CH_2)_3CH_3 + NaOH \rightarrow CH_3COONa + CH_3(CH_2)_3OH$ |
| Raimondi et al. (2014) | Experiment; Aqueous phase was extracted by secondary channels and concentration of acetone in aqueous phase was by UV-spectrophotometry | Aqueous phase: Water, Organic phase: toluene + acetone; During the droplet formation process, acetone transfers from toluene to water |
| Aoki et al. (2011) | Experiment; Extraction;<br>Concentration of phenol in aqueous phase was measured by UV-spectrophotometry measurements | Aqueous phase: Water; Organic phase: dodecane +phenol; During the droplet formation process, phenol transfers from dodecane to water |
| Matsuoka et al. (2016) | Experiment; Extraction; Concentration of phenol in organic phase was quantified by absorption photometry | Aqueous phase: water, Organic phase: Dodecane with 0.1 wt % phenol; During the droplet formation process, phenol transfers from dodecane to water |
| Woitalka et al. (2014) | Experiment; Extraction; Concentration of succinic acid in aqueous phase was subsequently analyzed based on acid–base titration | Aqueous phase: water, Organic phase: 1-butanol + succinic acid; During the droplet formation process, succinic acid transfers from 1-butanol to water |
| Darekar et al. (2014) | Experiment; Extraction | Aqueous phase: water + zinc sulfate, Organic phase: dodecane with 5% (v/v) D2EHPA |
| Bai et al. (2018) | Experiment; Concentration of Rhodamine B in Ionic liquid was measured by micro-LIF experiments | Aqueous phase: Ionic liquid ([C4mim][BF4]), Organic phase: toluene; Aqueous phase was injected in microchannels with two inlets, Rhodamine B was dissolved in one of the inlets; During the droplet formation process, Rhodamine B was redistribute and tend to uniform in droplets |

**Table 7** (continued)

| Ref. | Method | System and reaction |
|---|---|---|
| Özkan and Erdem (2015), Madadelahi et al. 2017 and Yang et al. (2018) | Simulation; Level set coupled with species transport model | Species/scalars/tracers are added into the dispersed phase, during the droplet formation process, scalars (species) redistribute and tend to uniform in droplets |
| Wang et al. (2015), Harshe et al. (2016), Qian et al. (2019b,c) | Simulation; VOF coupled with user defined scalar | |
| Zhao et al. (2012), (2015b) Qian et al. (2019c), Fu et al. (2016) | Simulation; Lattice Boltzmann coupled with passive tracer model | |

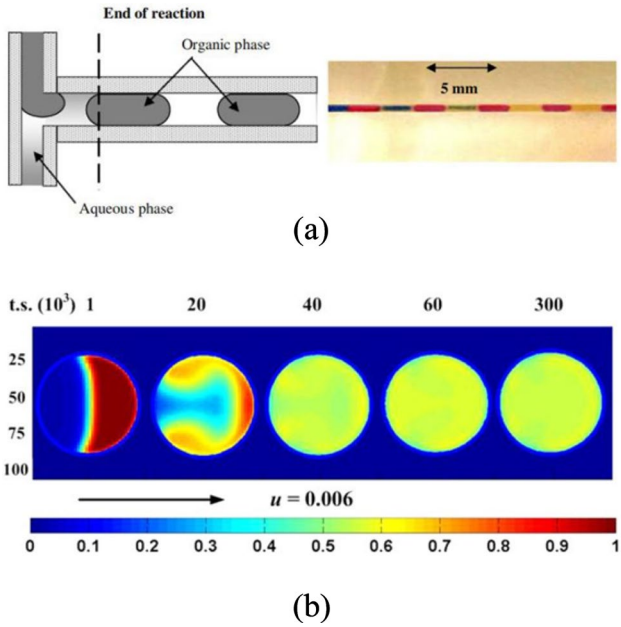


**Fig. 10** Visualization of mass transfer in droplet. **a** neutralization of $CH_3COOH$ with NaOH recorded by Dessimoz et al. (2008). The color change of aqueous phase from blue to yellow with droplet moving along the microchannel. **b** Dstribution of tracers in moving droplets recorded by Zhao et al. (2015) using LBM coupled with passive tracer model

acid–base titration. When conducting experiments without reaction, extraction is more often used for analyzing mass transfer efficiency (Raimondi et al. 2014; Woitalka et al. 2014; Kashid et al. 2007; Aoki et al. 2011; Matsuoka et al. 2016; Darekar et al. 2014). UV-spectrophotometry measurements are adopted for measuring the concentration of the extraction phase.

When conducting simulations involving reactions, 2D CFD is adopted. The aqueous phase and organic phase are represented by two adjacent units and the moving walls are set to replace the flow of the phases (Harries et al. 2003; Zhang et al. 2016; Sahu et al. 2016). However, most researches are conducted without reaction and the mass transfer efficiency is represented by the uniformity of species/scalars/tracers in droplets. Coupled methods including the level set coupled with species transport model, VOF coupled with user defined scalar and LBM coupled with passive tracer model are mostly used (Zhao et al. 2012; Özkan and Erdem 2015; Yang et al. 2018). Figure 10b presents distribution of tracers in droplets. It can be seen that with droplets moving along the microchannel, the distribution of tracers in droplets tends to be uniform.

For comparing mass transfer efficiency in different conditions, the overall volumetric mass transfer coefficient $k_L a$,

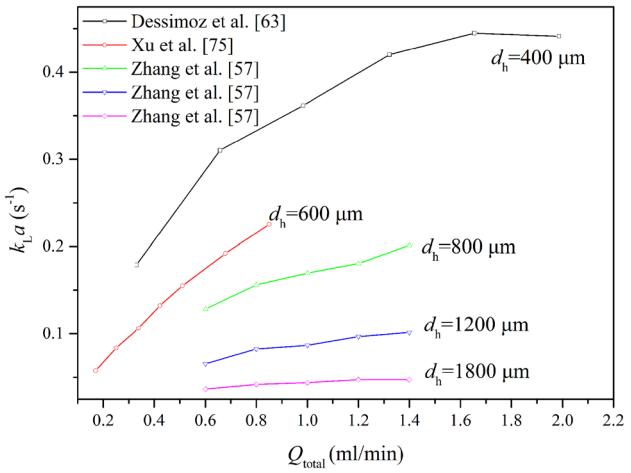


**Fig. 11** The overall volumetric mass transfer coefficient in microchannels with different dimensions

mixing index MI and intensity of segregation IOS are calculated and used for quantitative analysis.

$$k_{\mathrm{L}}a = \frac{1}{\tau}\ln\left(\frac{C^{*}_{\mathrm{aqu,in}} - C_{\mathrm{aqu,in}}}{C^{*}_{\mathrm{aqu,out}} - C_{\mathrm{aqu,out}}}\right), \tag{5}$$

where $\tau$ is the residence time, $C^{*}$ and $C$ are the equilibrium concentration of solute and concentration of solute, respectively. The subscripts in and out represent the inlet and outlet, respectively. The subscript aqu represents the aqueous phase. The solute is transformed from organic phase to aqueous phase.

$$\mathrm{MI} = \left(1 - \frac{\sqrt{\frac{1}{N}\sum_{i=1}^{N}\left(C_i - \overline{C}\right)^2}}{\overline{C}}\right) \times 100\%, \tag{6}$$

where $C_i$ is the arbitrary node concentration of the scalar, $\overline{C}$ is the concentration for which the mixing is achieved at ideal condition, $N$ is the number of nodes in the analyzed droplet. MI is the abbreviation of mixing index, which is defined based on the standard deviation from the ideal condition. The value of MI represents the uniformity of scalar distribution in the droplet.

$$\mathrm{IOS} = \left(\frac{C_{\sigma}^{2}}{\langle C\rangle - \langle 1 - \langle C\rangle\rangle}\right), \tag{7}$$

where $C, \langle C\rangle$ and $C_{\sigma}$ represent the normalized concentrations of fluids at each individual lattice, the statistical average value of $C$ in droplets and standard deviation, respectively. IOS is the abbreviation of intensity of segregation. The value of IOS represents the uniformity of the concentration distribution in droplets (Zhao et al. 2012).

## 3.3 Mass transfer efficiency in different conditions

### 3.3.1 Effect of microchannel features on mass transfer efficiency

For a specific two-phase system, microchannel features play an important role for mass transfer performance.

Generally, the microchannel with small dimensions performs better for enhancement of mass transfer efficiency (Ghaini et al. 2010; Xu et al. 2013; Raimondi et al. 2014; Matsuoka et al. 2016; Özkan and Erdem 2015). Figure 11 summarizes the overall volumetric mass transfer coefficient in microchannels with different dimensions. Although different liquid–liquid systems used, the influence of the microchannel dimension on the overall volumetric mass transfer coefficient is more remarkable.

The reduced microchannel dimension facilitates the droplet formed with a larger specific interfacial area and shortens the mass transfer length. Ghaini et al. (2010) studied effects of internal capillary diameter on mass transfer coefficient using both physical and chemical methods. Results indicated that decreasing the capillary diameter gave higher enhancement of the mass transfer coefficient. For example, $k_{\mathrm{L}}a$ was obtained for capillary diameters 1000 μm, 750 μm and 500 μm and the values were 1 s$^{-1}$, 1.28 s$^{-1}$ and 1.58 s$^{-1}$, respectively, at a constant aqueous phase flow rate of 70 ml/h. Xu et al. (2013) compared volumetric extraction rate in microchannels for a capillary diameters of 600 μm and 800 μm. The volumetric extraction rate in capillary diameter of 600 μm was always higher than for 800 μm. This was caused by the differences in specific interfacial areas between the phases. The mean interfacial area measured for the capillary diameter 600 μm was 4000 m$^2$/m$^3$, while for the capillary diameter 800 μm the value was only 3000 m$^2$/m$^3$. Raimondi et al. (2014) investigated mass transfer mechanism in microchannels with square cross section. The concentration profile of solute in dispersed phase along the microchannel was measured. Results showed that a smaller microchannel size provided a larger interfacial area, and accordingly a larger mass transfer coefficient. Matsuoka et al. (2016) studied effects of the hydraulic diameter on mass transfer efficiency. Circular and semicircular microchannels with a hydraulic equivalent diameter range of 600 μm to 2000 μm were designed to perform liquid–liquid extraction of phenol from dodecane to water. At the same Reynolds number, volumetric mass transfer coefficient increased with the decrease of hydraulic equivalent diameter both in circular and semicircular microchannels.

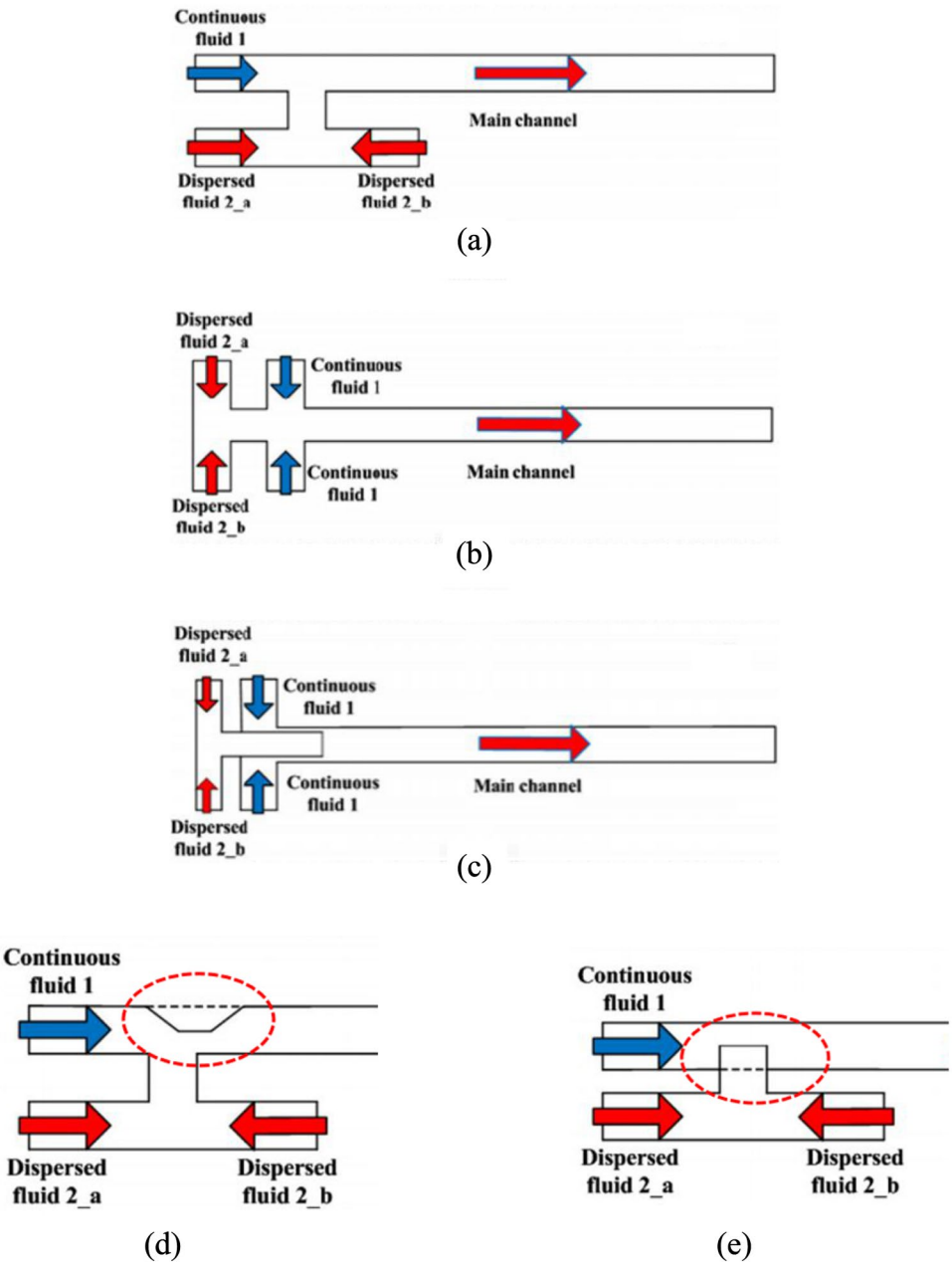


**Fig. 12** Configurations of inlet junction designed by Zhao et al. (2012). **a** T-junction; **b** cross-shape microchannel; **c** coaxial micro-capillary; **d** modified T-junction with venturi-shape; **e** micro-capillary insertion microchannel

Microchannel structures including configurations of inlet junction and configurations of the main channel are most important for enhancement of mass transfer efficiency.

Configurations of inlet junction mainly affect the mass transfer efficiency in the droplet formation process. Kashid et al. (2011) conducted experiments to identify the mass transfer efficiency in different microchannels including T-square, T-trapezoidal, Y-rectangular, concentric and caterpillar as shown in Fig. 2. It is worth noting that the caterpillar microchannel was a microchannel with internal bas-relief structure and the other four microchannels had no internal structures. By changing the water flow rate, the mass transfer coefficient in each microchannel was obtained and plotted. Results showed that the caterpillar microchannel had best performance due to its internal bas-relief structure. The existence of the internal bas-relief structure created a considerably fine dispersion and provided a higher interfacial area compared with other microchannels. Compared with non-structured microchannels, the mass transfer coefficient in caterpillar microchannel was almost 1 order of magnitude higher than the concentric microchannel and 2–3 times higher than that of on the other microchannels. Zhao et al. (2012) compared mass transfer efficiency in different configurations of the inlet junction including T-junction, cross-shaped junction and coaxial micro-capillary as shown in Fig. 12a–c. The LBM method was adopted in the

simulations. Results showed that in cross-shaped junction microchannel and micro-capillary microchannel, the velocity field and concentration distribution were both kept symmetric in the droplet formation process. This made the tracers difficult to distribute uniformly and caused lower mass transfer efficiency. For breaking up the bilateral symmetry, modified T-junction with venturi-shape and micro-capillary insertion microchannel were proposed as shown in Fig. 12d–e. The modified structures performed well for enhancement of mass transfer efficiency. When droplet moves through the microchannel, distribution of the tracers was reorientated due to the asymmetric inner circulation which was disturbed by the venturi-shape structure and micro-capillary insertion structure. Sattari-Najafabadi et al. (2017) compared effects of two aspect ratios (ratio of the width to the depth of microchannel) and three configurations of the inlet junction which includes cross-shaped junction, crossed-shaped T-junction and opposed T-junction on mass transfer efficiency in liquid–liquid droplet flow. Results showed that a longer droplet length, which was formed in microchannel with an aspect ratio two, induced a growth of the stagnant zone and a decline of the wall renewal. Thus, mass transfer efficiency in the microchannel with aspect ratio two was lower than in microchannel with an aspect ratio one. Also, comparing configurations of the inlet junction revealed that cross-shaped junction had better performance than cross-shaped T-junction and opposed T-junction. This is because in cross-shaped junction, continuous phase was in contact with the dispersed phase from both sides; while in other configurations, the continuous phase touched the dispersed phase only from one side. In addition, the authors extended the experiments to study the effect of hydraulic diameters on mass transfer efficiency (Sattari-Najafabadi et al. 2017b). The microchannels were designed with hydraulic diameters of 200 µm, 400 µm and 600 µm. The calculated mass transfer coefficients in three microchnnels revealed that with decreasing hydraulic diameter, the mass transfer efficiency was remarkably increased. On average, the overall mass transfer coefficients were promoted by 112.2% and 124.4% the hydraulic diameter was reduced from 600 µm to 400 µm and 400 µm to 200 µm, respectively.

Configurations of the main channel have a dominating effect when the droplet is moving along the microchannel. Curvature-based microchannel and obstacle-based microchannel are the two main types used for enhancement of mass transfer efficiency when a droplet is moving along the microchannel (Plouffe et al. 2016a, b; Woitalka et al. 2014; Aoki et al. 2011; Darekar et al. 2014; Özkan and Erdem 2015; Yang et al. 2018; Zhao et al. 2015b; Malsch et al. 2008). When a droplet is moving along the microchannel, the changing microchannel structure disturbed the fluid flow and broke up the symmetrical inner circulation in the droplets. Thus, the mass transfer efficiency was greatly enhanced.

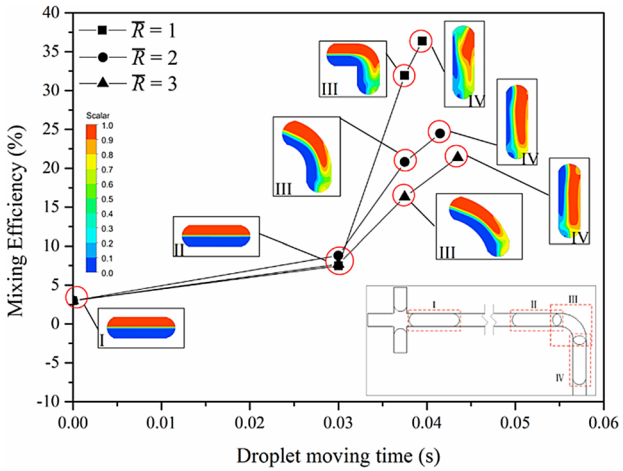


**Fig. 13** Variations of mass transfer efficiency before and after the droplet across the serpentine section (Qian et al. 2019b)

Figure 13 presents the variations of the mass transfer efficiency before and after the droplet across the serpentine section (Qian et al. 2019a). It can be seen that before the droplet across the serpentine section, the mass transfer efficiency is about 7% ~ 8%. However, the mixing efficiency reaches 36% when the droplet moves out of the turn. The results quantified the effect of the main channel structure on the mixing process.

The serpentine section promotes the mass transfer efficiency significantly due to the deformed inner circulation in droplet. Figure 14 presents the inner circulation in droplets observed in straight microchannel and curvature-based microchannel (Malsch et al. 2008). It can be seen obviously that droplets moving along the straight microchannel have an axially symmetric inner circulation. The symmetric inner circulation obstructs the concentration redistribution in the radial direction. In contrast, in the curvature-based microchannel, the inner circulation is asymmetric and enables the concentration gradient to be more uniform.

Nonino et al. (2009) designed zig-zag, curvilinear and square-wave microchannels with square cross section. Simulations were conducted to determine the mass transfer efficiency in each microchannel and comparisons were made with straight microchannels. The mass transfer efficiency was plotted as a function of Reynolds number. In all microchannels, curvilinear and square-wave microchannels presented better mass transfer efficiency than zig-zag microchannels. Aoki et al. (2011) examined extraction rate in microchannels with expansion and contraction structure as shown in Fig. 15. Results showed that at a constant total flow rate, 10 ml/min and 20 ml/min, the extraction rate in the microchannel with expansion structure was higher than the one with contraction structure. The authors further studied the relationship between location of the expansion structure

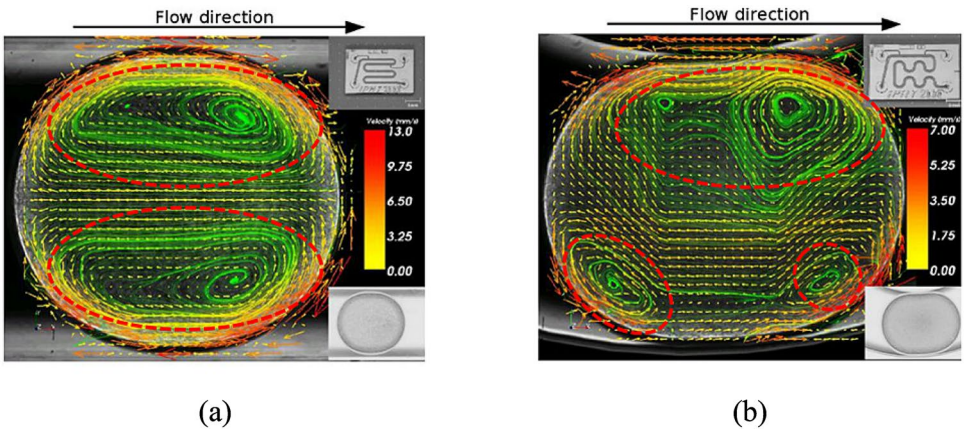


**Fig. 14** Inner circulation in droplets recorded by Malsch et al. (2008). **a** Symmetric inner circulation in droplet observed in straight microchannel; **b** asymmetric inner circulation in droplet observed in curvature-based microchannel

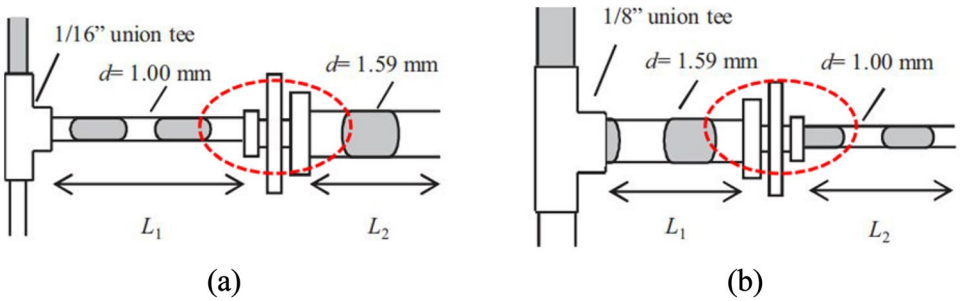


**Fig. 15** Microchannels designed by Aoki et al. (2011). **a** Microchannels with expansion structure; **b** microchannels with contraction structure

and the extraction rate. The maximum efficiency was achieved in the specific location of the expansion near the outlet. The results also indicated that with a sudden change of the microchannel dimension near the outlet can re-activate the inner circulation in droplets which may contribute to the improved mass transfer efficiency. Darekar et al. (2014) carried out extraction experiments to quantify the overall mass transfer coefficient for various conditions. A T-junction serpentine microchannel and a split and recombine microchannel were used in the experiments as shown in Fig. 16. The overall mass transfer coefficient in the two microchannels was compared at the same residence time, the same Reynolds number and the same average velocity. Results showed that only at the same residence time, the mass transfer coefficient in the T-junction serpentine microchannel was higher than in the split and recombine microchannels. At the same Reynolds number and the same average velocity, the split and recombine microchannels had better performance. The authors suggested that comparison of mass transfer efficiency based on average velocity was more reasonable. This was argued as the average velocity is directly linked to the energy dissipation which is another important index for evaluation of the systems. Özkan and Erdem (2015) conducted simulations to identify the mass transfer efficiency in sinusoidal microchannels as shown in Fig. 17. Mass transfer efficiency in six different microchannels including various channel curvature and cross section area was calculated. Results showed that microchannels with smaller radius and smaller cross section area provided higher mass transfer efficiency. The decreased microchannel size provided wider dispersion length difference, more frequent velocity change and vertical trajectory variation of particles. All of these were greatly enhancing the mass transfer efficiency. Plouffe et al. (2016a, b) conducted experiments to study mass transfer efficiency in various microchannels which were named SZ, TG, Venturi, Sickle and Spade as shown in Fig. 5. It is worth noting that not the overall mass transfer coefficients were compared in different microchannels but the Damköhler numbers were compared. Based on different Damköhler numbers, the best and the worst mass transfer rates were achieved by the Sickle microchannel and TG microchannels, respectively.

In addition, microchannel structures which promote the mass transfer efficiency both in the droplet formation process and droplet movement along the microchannel have been proposed. Bai et al. (2018) performed experiments for analyzing the mass transfer efficiency in cross-shaped microchannel. However, due to the high viscosity and small diffusion coefficient of the ionic liquid, which was used in their experiment, the cross-shaped microchannel presented poor mass transfer efficiency. To enhance the mass transfer efficiency, two methods were adopted by the author. One method was to change the way of droplet formation, and accordingly the cross-shaped junction microchannel was

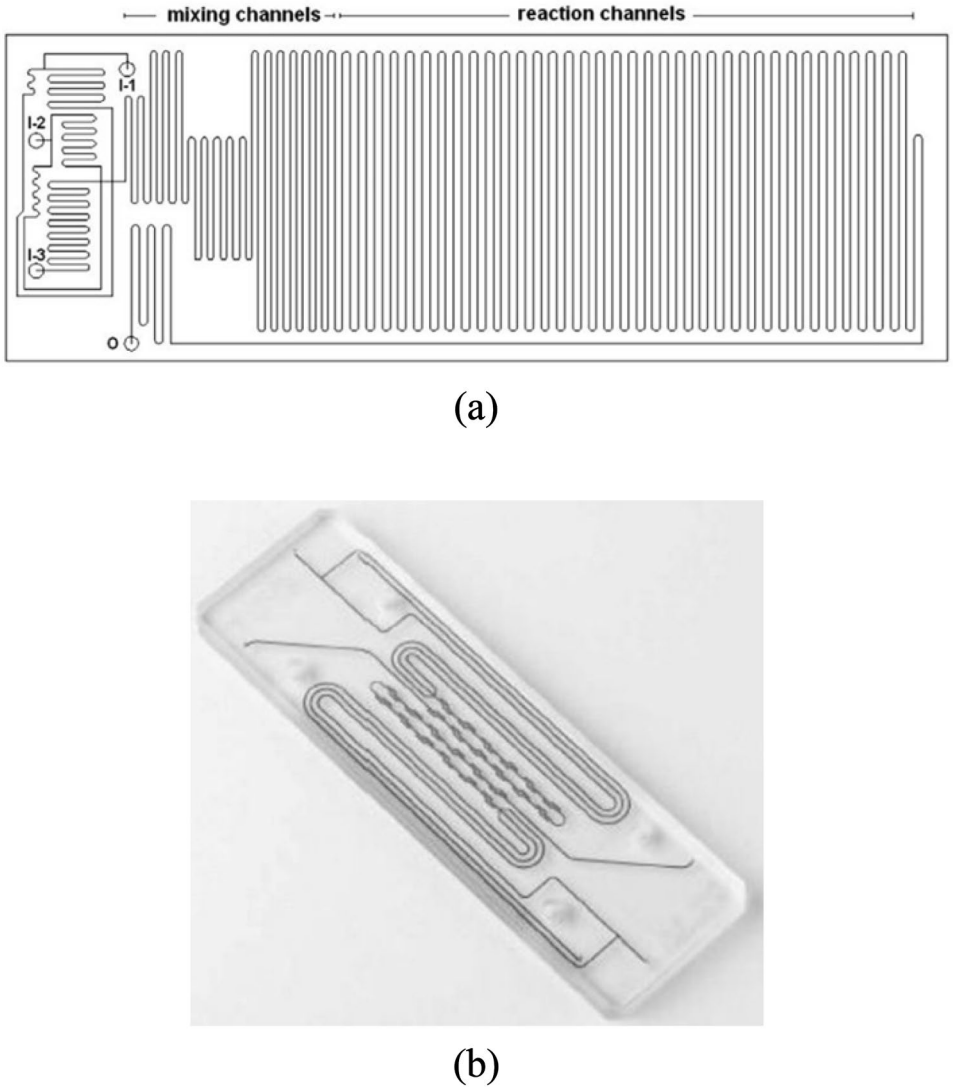


**Fig. 16** Microchannels designed by Darekar et al. (2014). **a** T-junction serpentine microchannel; **b** split and recombine microchannel

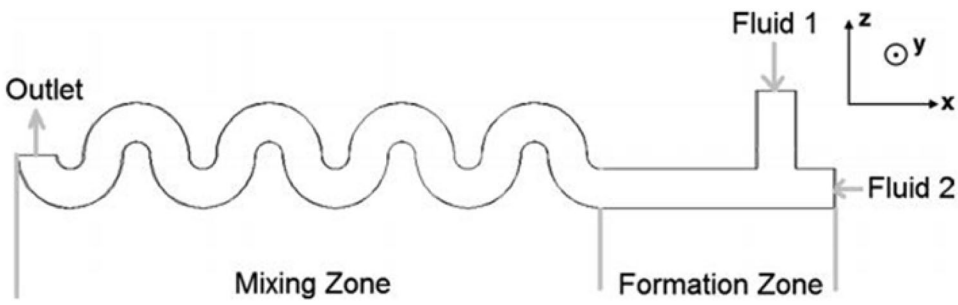


**Fig. 17** Microchannels designed by Özkan and Erdem (2015)

replaced by T-junction and Y-junction. The other method was to change the way of droplet movement along the microchannel, and then the straight microchannel was replaced by meandering microchannel and deforming microchannel. Finally, the authors combined the two methods and proposed the Y-deforming microchannel for achieving excellent mass transfer performance. The combined structure also was adopted by Yang et al. (2018). The authors studied the mass transfer efficiency in T-junction microchannel and sinusoidal microchannel, respectively. Based on the results, an optimized microchannel structure was proposed which combined a T-junction inlet with a sinusoidal microchannel. This optimized structure combined twirling effect, dean

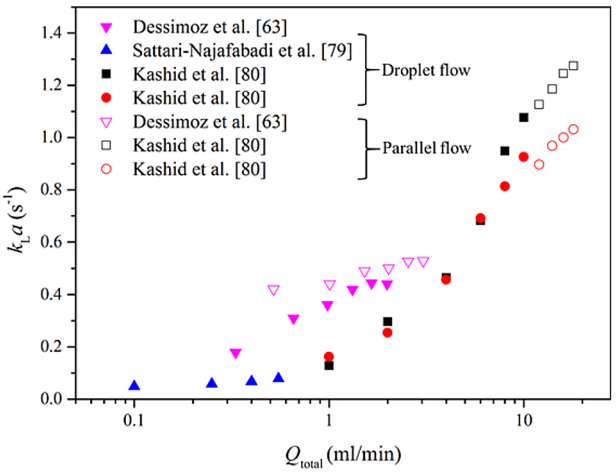


**Fig. 18** The overall volumetric mass transfer coefficient in function of the total flow rate ($Q_d = Q_c$)

vortices and droplet deformation effect together. Thus, the mass transfer efficiency was significantly promoted.

### 3.3.2 Effect of flow rate

The increase of the total flow rate leads to an increase of the droplet velocity. With higher droplet velocity, the intensification of the inner circulation is more pronounced and the mass transfer efficiency is significantly improved. Figure 18 summarizes the over volumetric mass transfer coefficient as a function of the total flow rate in published literatures which all have the same hydraulic diameter of 400 μm. It can be seen that with an increase of the total flow rate, the overall volumetric mass transfer coefficient increases accordingly whether in the droplet regime or the parallel regime. However, it should be emphasized that in the droplet flow regime, the overall volumetric mass transfer coefficient increases with a high rate. When transiting to the parallel regime, the rate of increase reduces. This highlights the superiority of the droplet in mass transfer performance due to the specific interfacial area and intense inner circulation.

In addition, it can be seen from Fig. 18 that the overall volumetric mass transfer coefficient measured by Dessimoz et al. (2008) is much higher than that measured by Sattari-Najafabadi et al. (2017), although the same liquid (hexane)–liquid (water) system is used in their experiment. Two possible reasons may be the amount of the acid contained in the oil phase and the deviation induced by the specific interfacial area. In experiment conducted by Sattari-Najafabadi et al. (2017), the organic phase was n-hexane with 0.5 M acetic acid. While in experiment conducted by Dessimoz et al. (2008), the organic phase was n-hexane containing 0.6 M trichloroacetic acid. The increase of the acid concentration led to the decrease of the interfacial tension. The increased interfacial movement promoted the mass transfer process. Moreover, according to Sattari-Najafabadi et al. (2017), the droplet cap was considered as two hemispheres with the radius equal to the microchannel width. However, the radius of droplet cap in Dessimoz et al. (2008) was calculated by the Brethertons law (Bretherton 1961). The differences induced the relative error for calculating the specific interfacial area which directly led to the deviation on the overall volumetric mass transfer coefficient.

Moreover, at constant total flow rate, the dispersed phase fraction $\varepsilon_d$ ($0 < \varepsilon_d < 1$), which is defined as Eq. (8), has an effect on mass transfer efficiency.

$$\varepsilon_{\mathrm{d}} = \frac{u_{\mathrm{d}}}{u_{\mathrm{total}}}, \tag{8}$$

where $u_{\mathrm{d}}$ and $u_{\mathrm{total}}$ represent the dispersed phase velocity and total velocity, respectively. It should be noted that the no-slip velocity between phases is assumed when using Eq. (8). Generally, the actual droplet velocity is higher than the total velocity (Salim et al. 2008; Darekar et al. 2014; Yagodnitsyna et al. 2016).The increase of the dispersed phase fraction leads to an increase of the droplet length. The maximum mass transfer efficiency only achieved at a suitable droplet length. Tice et al. (2003) studied the relationship between droplet length and mass transfer efficiency experimentally. The droplet was set to move along the microchannel with a constant velocity of 50 mm/s. Different droplet length was achieved by adjusting the dispersed phase fraction. For analysis of the mass transfer efficiency, marker was added in dispersed phase and the uniformity of the marker concentration in droplets was measured. Results showed that the maximum mass transfer efficiency was achieved at the dispersed phase fraction 0.3. In addition, Wang et al. (2015) carried out simulations to study the relationship between droplet length and mass transfer efficiency. Results showed that only for the dimensionless droplet length less than 2, fast mixing could be achieved. The best mass transfer efficiency was obtained when the droplet length was comparable with the microchannel width. In the research conducted by Qian et al. (2019), the dimensionless droplet lengths were all higher than two, while the fast mixing was also achieved. This was mainly caused due to the selection of the cross-shaped junction and the initial distribution of the dispersed phase and the continuous phase. For most researches using the cross-shaped junction, the dispersed phase and the continuous phase are injected in the microchannel through the horizontal channel and the vertical channel, respectively (Cao et al. 2018; Sattari-Najafabadi et al. 2017a; Bai et al. 2018). However, the initial distribution of the dispersed phase and continuous phase presented in Ref. (Qian et al. 2019c) was totally opposite. The dispersed phase was injected through the vertical inlet and the continuous phase was injected into the microchannel through the horizontal one. This approach

**Table 8** Relative error between the data obtained in experiments and data predicted by Eqs. (9) to (12) (Eain et al. 2015)

| Continuous phase–dispersed phase | Without film (%) | With film (%) | | |
|---|---|---|---|---|
| | Equation (9) | Equation (10) | Equation (11) | Equation (12) |
| Pd5–water | 154.9–417.1 | 2.1–48.9 | 3.7–60.8 | 3.5–60.9 |
| Dodecane–water | 79.4–518.1 | 18.2–74.7 | 85.7–307.3 | 85.5–306.7 |
| FC40–water | 68.6–365.3 | 5.3–54.9 | 17.6–61.5 | 17.9–61.6 |
| AR20–water | 76.1–420.8 | 2.5–28.7 | 2.5–31.1 | 2.5–30.9 |

made the best use of the inner circulation when the droplet moving through the microchannel. Therefore, the best mass transfer performance can be achieved without restriction the droplet length.

### 3.4 Energy dissipation

An ideal condition for enhancement of mass transfer performance should consider not only the mass transfer efficiency but also the energy dissipation. Thus, the balance between mass transfer efficiency and energy dissipation should be considered seriously. Pressure drop is adopted as an indicator for the assessment of energy dissipation (Nonino et al. 2009; Lemenand et al. 2013). The higher velocity, the more complex structure of microchannels and the smaller microchannel dimensions all lead to a higher pressure drop. Salim et al. (Salim et al. 2008) investigated water–oil two-phase flows in microchannels with two different hydraulic diameters. Pressure drops at various flow rates were measured using the homogeneous and Lockhart–Martinelli models. Results indicated that pressure drops depend closely on the flow rates, the phase which was the first injected and microchannel material. When oil was saturated initially in microchannels, the pressure drop increased at low water superficial velocities and then decreased sharply. After the water superficial velocities exceeded 10 cm/s, the pressure drop increased almost linearly with water superficial velocities. However, with water initially saturated in microchannels, the pressure drop always increased with oil superficial velocity. Similar results were also found by Tsaoulidis et al. (2013). Kashid and Agar (2007) carried out experiments to study the hydrodynamics of water–cyclohexane two-phase flow. Pressure transducers were placed at the inlet and downstream of the microchannel to record the pressure variation for the two-phase flow. Pressure behaviors observed at different droplet velocities and capillary dimensions were plotted. Results indicated that the pressure drop increased with increasing droplet velocity and decreasing capillary dimensions. Furthermore, correlations were proposed for pressure drop predictions along the microchannel as shown in Eqs. (9) and (10).

$$\Delta P_{\mathrm{WOF}} = \frac{L}{L_{\mathrm{U}}}\left(\left[\frac{8u_{\mathrm{d}}v\alpha L_{\mathrm{U}}}{R^2}\right] + \left\{\frac{8u_{\mathrm{c}}v(1-\alpha)L_{\mathrm{U}}}{R^2}\right\}\right) + \frac{2L-L_{\mathrm{U}}}{L_{\mathrm{U}}}\left\langle\frac{2\sigma}{R}\cos\theta\right\rangle, \tag{9}$$

$$\left(\frac{\Delta P}{L}\right)_{\mathrm{WF}} = \left(\frac{\alpha}{1-((R-h)/R)^4}\right)\left(\frac{\Delta P}{L}\right)_{\mathrm{c}}, \tag{10}$$

where $L$, $L_{\mathrm{U}}$, $R$ and $h$ represent the capillary length, droplet unit length, radius of capillary and film thickness, respectively. $\mu$ and $\sigma$ represent the fluid viscosity and interfacial tension. $v$ and $\alpha$ represent the droplet velocity and dispersed phase length fraction, respectively. $\theta$ represents the contact angle. $\Delta P_{\mathrm{WOF}}$ and $\Delta P_{\mathrm{WF}}$ represent the pressure drop without film and pressure drop with film, respectively. Comparing with data collected in the experiment, the correlation with a film showed a better agreement. Jovanovic et al. (2011) studied the pressure drop in water–toluene and ethylene glycol/water–toluene systems. Two models, which were called stagnant film model and moving film model, were proposed for predicting the pressure drop.

$$\Delta P_{\mathrm{SF}} = \left[\frac{8u_{\mathrm{d}}v\alpha L}{(R-h)^2}\right] + \left\{\frac{8u_{\mathrm{c}}v(1-\alpha)L}{R^2}\right\} + \left\langle\frac{L}{L_{\mathrm{U}}}7.16(3Ca)^{2/3}\frac{\sigma}{d}\right\rangle, \tag{11}$$

$$\Delta P_{\mathrm{MF}} = \left[\frac{4v\alpha L}{\left(R^2-(R-h)^2\right)/u_{\mathrm{c}} + 0.5(R-h)^2/u_{\mathrm{d}}}\right] + \left\{\frac{8u_{\mathrm{c}}v(1-\alpha)L}{R^2}\right\} + \left\langle\frac{L}{L_{\mathrm{U}}}7.16(3Ca)^{2/3}\frac{\sigma}{d}\right\rangle, \tag{12}$$

where $L$, $L_{\mathrm{U}}$, $R$, $d$ and $h$ represent the capillary length, droplet unit length, radius of capillary, diameter of capillary and film thickness, respectively. $\mu$ and $\sigma$ represent the fluid viscosity and interfacial tension. $v$ and $\alpha$ represent the droplet velocity and dispersed phase length fraction, respectively. $\theta$ represents the contact angle. $\Delta P_{\mathrm{SF}}$ and $\Delta P_{\mathrm{MF}}$ represent the pressure drop with stagnant film and pressure drop with moving film, respectively. The models were compared with the liquid–liquid pressure drop studies found in literature. Finally, the stagnant film model was found to be more adequate to predict pressure drop. The proposed models in Kashid and Agar (2007) and Jovanovic et al. (2011) both considered that the pressure drop across the length of the capillary comprised three parts: pressure drop caused by the dispersed phase expressed in Eqs. (9), (11) and (12) by the first term, the pressure drop caused by the continuous

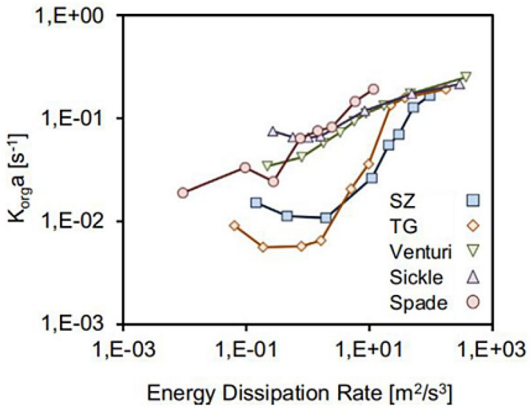


**Fig. 19** Overall volumetric mass transfer coefficients in different microchannels in n-butanol/aqueous NaOH system plotted by Plouffe et al. (2016)

phase expressed in Eqs. (9), (11) and (12) by the second term and pressure drop caused by the interface expressed in Eqs. (9), (11) and (12) by the third term.

To validate the accuracy of the pressure drop models proposed by Kashid and Agar (2007) and Jovanovic et al. (2011), Eain et al. (2015) conducted comprehensive experiments in different liquid–liquid two-phase systems which included a wide range of Reynolds number, $1.45 < Re < 97.48$, and Capillary number, $4.49 \times 10^{-5} < Ca < 0.0098$. Table 8 presents the summary of the relative error between the experimental data obtained in different systems and data predicted by Eqs. (9) to (12).

It can be seen that the data predicted by the model without film, Eq. (9), greatly deviate the experimental data due to the assumption of without film. In this assumption, the contact angle is considered to be constant when the droplet across the microchannel. Moreover, data predicted by two models, Eqs. (11) and (12), show a highly similarity. This is attributed to the assumption that the pressure drop caused by the continuous phase and the interface account for over 90% of the total pressure drop. While the two terms in Eqs. (11) and (12) keep the same. Finally, Eain et al. (2015) pointed out that none of the proposed models gave a relatively accurate prediction within ± 15% of the relative error. The main problem lies in the methods used to predicted the interface pressure drop.

Based on pressure drop, the energy dissipation rate can be quantified as shown in Eq. (13).

$$\varepsilon_{\Delta P} = \frac{u \Delta P}{\rho L}. \tag{13}$$

Plouffe et al. (2016) plotted the overall mass transfer coefficients versus the energy dissipation rate as shown in Fig. 19. It is obvious that higher mass transfer efficiency is always accompanied by a higher energy dissipation.

## 4 Conclusion

Extensive efforts have been made for exploring the hydrodynamics of liquid–liquid two-phase flow in microchannels and promoting its industrial applications. However, there are still many aspects deserve to be considered in further research.

Liquids involved in experiments and simulations are mainly Newtonian liquids. Thus, researches focused on non-Newtonian liquids should be performed for a comprehensive understanding of liquid–liquid two-phase flow; Experiments and simulations are carried out mostly at room temperature. However, some liquid properties are highly sensitive to temperature. Thus, variation of temperature should be considered; Researches on liquid–liquid two-phase flow are widely studied; while, the uniform criteria such as for distinguishing the flow pattern transition and predicting the droplet characteristic are still inadequate. Thus, data at different conditions should be collected and databases should be set up. Scaling laws and general correlations need to be proposed.

The inner circulations existed in a droplet can be divided into two parts: the main circulation which is induced by the interaction with the wall and the minor circulation which is induced by the interaction with the continuous phase. Whether the correlations are existed between two-circulation path and the droplet length may deserve to further consider. In addition, the film thickness plays a significant role to calculate the specific interfacial area. Although the widely use of the Brethertons law, methods for determining the film thickness need to be further developed.

Simulations performed for studying the mass transfer performance in liquid–liquid two-phase flow mainly adopt non-reaction systems and the mass transfer efficiency is represented by the distribution uniformity of tracers/species/scalars in droplets. No better guidance is provided when reactions are involved. Thus, more effective simulation methods should be developed to better adopt actual working conditions; Mass transfer performance is widely studied in stable flow patterns such as droplet flow and parallel flow. However, in actual working conditions, flexible flow conditions may increase the instability of fluid flow and cause different flow patterns. Thus, mass transfer performance in transition flow patterns should be studied.

Energy dissipation is an important parameter for evaluating the overall efficiency of a microfluidic system and it has been widely studied in turbulent flow. However, in laminar flow, there are less reports. Researches should be extended further to determine the balance between energy dissipation and mass transfer efficiency. In addition, when droplets moving through the microchannel, it can be analogous to an electric circuit and the droplet can be considered as the resistance. In a particular microchannel length, the pressure

drop may be influenced by not only the droplet length and droplet unit length, but also the numbers of droplet. This question needs to be further clarified.

**Acknowledgements** This work is supported by the National Natural Science Foundation of China through Grant No. 51805470, the Youth Funds of the State Key Laboratory of Fluid Power and Mechatronic Systems (Zhejiang University) through Grant No. SKLoFP-QN-1801, and the Fundamental Research Funds for the Central Universities through Grant No. 2018QNA4013.

## References

Antony R, Nandagopal MSG, Sreekumar N, Rangabhashiyam S, Selvaraju N (2014) Liquid-liquid slug flow in a microchannel reactor and its mass transfer properties—a review. Bull Chem React Eng Catal 9:207–223. https://doi.org/10.9767/bcrec.9.3.6977.207-2

Aoki N, Tanigawa S, Mae K (2011) A new index for precise design and advanced operation of mass transfer in slug flow. Chem Eng J 167:651–656. https://doi.org/10.1016/j.cej.2010.07.071

Bai L, Fu Y, Yao M, Cheng Y (2018) Enhancement of mixing inside ionic liquid droplets through various micro-channels design. Chem Eng J 332:537–547. https://doi.org/10.1016/j.cej.2017.09.086

Bashir S, Rees JM, Zimmerman WB (2011) Simulations of microfluidic droplet formation using the two-phase level set method. Chem Eng Sci 66:4733–4741. https://doi.org/10.1016/j.ces.2011.06.034

Bretherton FP (1961) The motion of long bubbles in tubes. J Fluid Mech 10:166–188. https://doi.org/10.1017/S0022112061000160

Burns J, Ramshaw C (2001) The intensification of rapid reactions in multiphase systems using slug flow in capillaries. Lab Chip 1:10–15. https://doi.org/10.1039/b102818a

Cai G, Xue L, Zhang H, Lin J (2017) A review on micromixers. Micromachines 8:274. https://doi.org/10.3390/mi8090274

Cao J, Krause K, Kothe E, Martin K, Roth M, Köhler JM (2013) Application of micro-segmented flow for two-dimensional characterization of the combinatorial effect of zinc and copper ions on metal-tolerant streptomyces strains. Appl Microbiol Biotechnol 97:8923–8930. https://doi.org/10.1007/s00253-013-5147-8

Cao Z, Wu Z, Sundén B (2018) Dimensionless analysis on liquid-liquid flow patterns and scaling law on slug hydrodynamics in cross-junction microchannels. Chem Eng J 344:604–615. https://doi.org/10.1016/j.cej.2018.03.119

Cate DM, Adkins JA, Mettakoonpitak J, Henry CS (2015) Recent developments in paper-based microfluidic devices. Anal Chem 87:19–41. https://doi.org/10.1021/ac503968p

Chen C, Zhao Y, Wang J, Zhu P, Tian Y, Xu M (2018) Passive mixing inside microdroplets. Micromachines 9:160. https://doi.org/10.3390/mi9040160

Chiarello E, Derzsi L, Pierno M, Mistura G, Piccin E (2015) Generation of oil droplets in a non-newtonian liquid using a microfluidic T-junction. Micromachines 6:1825–1835. https://doi.org/10.3390/mi6121458

Chinnov EA, Ron'Shin FV, Kabov OA (2015) Regimes of two-phase flow in micro- and minichannels (review). Thermophys Aeromech 22:265–284. https://doi.org/10.1134/S0869864315030014

Christopher GF, Anna SL (2007) Microfluidic methods for generating continuous droplet streams. J Phys D 40:R319–R336. https://doi.org/10.1088/0022-3727/40/19/R01

Cristini V, Tan Y (2004) Theory and numerical simulation of droplet dynamics in complex flows-a review. Lab Chip 4:257–264. https://doi.org/10.1039/b403226h

Cubaud T, Mason TG (2008) Capillary threads and viscous droplets in square microchannels. Phys Fluids 20:053302. https://doi.org/10.1063/1.2911716

Darekar M, Sen N, Singh KK, Mukhopadhyay S, Shenoy KT, Ghosh SK (2014) Liquid-liquid extraction in microchannels with zinc-d2ehpa system. Hydrometallurgy 144–145:54–62. https://doi.org/10.1016/j.hydromet.2014.01.010

Darekar M, Singh K, Mukhopadhyay S, Shenoy K (2017) Liquid-liquid two-phase flow patterns in Y-junction microchannels. Ind Eng Chem Res 56:12215–12226. https://doi.org/10.1021/acs.iecr.7b03164

De Menech M, Garstecki P, Jousse F, Stone HA (2008) Transition from squeezing to dripping in a microfluidic T-shaped junction. J Fluid Mech 595:141–161. https://doi.org/10.1017/S002211200700910X

Derzsi L, Kasprzyk M, Plog JP, Garstecki P (2013) Flow focusing with viscoelastic liquids. Phys Fluids 25:092001. https://doi.org/10.1063/1.48179

Dessimoz A-L, Cavin L, Renken A, Kiwi-Minsker L (2008) Liquid-liquid two-phase flow patterns and mass transfer characteristics in rectangular glass microreactors. Chem Eng Sci 63:4035–4044. https://doi.org/10.1016/j.ces.2008.05.005

Dore V, Tsaoulidis D, Angeli P (2012) Mixing patterns in water plugs during water/ionic liquid segmented flow in microchannels. Chem Eng Sci 80:334–341. https://doi.org/10.1016/j.ces.2012.06.030

Eain MM, Egan V, Howard JA, Walsh P, Walsh EJ, Punch J (2015) Review and extension of pressure drop models applied to Taylor flow regimes. Int J Multiph Flow 68:1–9. https://doi.org/10.1016/j.ijmultiphaseflow.2014.09.006

Feigl K, Tanner FX, Holzapfel S, Windhab EJ (2014) Effect of flow type, channel height, and viscosity on drop production from micro-pores. Chem Eng Sci 116:372–382. https://doi.org/10.1016/j.ces.2014.05.015

Fries DM, Voitl T, Von Rohr PR (2008) Liquid extraction of vanillin in rectangular microreactors. Chem Eng Technol 31:1182–1187. https://doi.org/10.1002/ceat.200800169

Fu T, Wu Y, Ma Y, Li HZ (2012) Droplet formation and breakup dynamics in microfluidic flow-focusing devices: from dripping to jetting. Chem Eng Sci 84:207–217. https://doi.org/10.1016/j.ces.2012.08.039

Fu T, Wei L, Zhu C, Ma Y (2015) Flow patterns of liquid-liquid two-phase flow in non-Newtonian fluids in rectangular microchannels. Chem Eng Process 91:114–120. https://doi.org/10.1016/j.cep.2015.03.020

Fu Y, Bai L, Zhao S, Bi K, Jin Y, Cheng Y (2016) Droplet in droplet: LBM simulation of modulated liquid mixing. Chem Eng Sci 155:428–437. https://doi.org/10.1016/j.ces.2016.08.035

Garstecki P, Fuerstman MJ, Stone HA, Whitesides GM (2006) Formation of droplets and bubbles in a microfluidic T-junction—scaling and mechanism of break-up. Lab Chip 6:437–446. https://doi.org/10.1039/b510841a

Ghaini A, Kashid MN, Agar DW (2010) Effective interfacial area for mass transfer in the liquid–liquid slug flow capillary microreactors. Chem Eng Process Process Intensif 49:358–366. https://doi.org/10.1016/j.cep.2010.03.009

Gu H, Duits MH, Mugele F (2011) Droplets formation and merging in two-phase flow microfluidics. Int J Mol Sci 12:2572–2597. https://doi.org/10.3390/ijms12042572

Gupta A, Kumar R (2010a) Effect of geometry on droplet formation in the squeezing regime in a microfluidic T-junction. Microfluid Nanofluid 8:799–812. https://doi.org/10.1007/s10404-009-0513-7

Gupta A, Kumar R (2010b) Flow regime transition at high capillary numbers in a microfluidic T-junction: viscosity

contrast and geometry effect. Phys Fluids 22:122001. https://doi.org/10.1063/1.3523483
Harries N, Burns J, Barrow DA, Ramshaw C (2003) A numerical model for segmented flow in a microreactor. Int J Heat Mass Tran 46:3313–3322. https://doi.org/10.1016/S0017-9310(03)00120-0
Harshe Y, Eijk MV, Kleijn CR, Kreutzer MT, Boukany PE (2016) Scaling of mixing time for droplets of different size traveling through a serpentine microchannel. Rsc Advances 6:98812–98815. https://doi.org/10.1039/c6ra17728j
He P, Barthesbiesel D, Leclerc E (2010) Flow of two immiscible liquids with low viscosity in Y shaped microfluidic systems: effect of geometry. Microfluid Nanofluid 9:293–301. https://doi.org/10.1007/s10404-009-0546-y
Jovanovic J, Zhou W, Rebrov EV, Nijhuis TA, Hessel V, Schouten JC (2011) Liquid-liquid slug flow: hydrodynamics and pressure drop. Chem Eng Sci 66:42–54. https://doi.org/10.1016/j.ces.2010.09.040
Karadimitriou NK, Hassanizadeh SM (2012) A review of micromodels and their use in two-phase flow studies. Vadose Zone J 11:215–228. https://doi.org/10.2136/vzj2011.0072
Kashid MN (2005) Internal circulation within the liquid slugs of a liquid-liquid slug-flow capillary microreactor. Ind Eng Chem Res 44:5003–5010. https://doi.org/10.1021/ie0490536
Kashid MN, Agar DW (2007) Hydrodynamics of liquid–liquid slug flow capillary microreactor: flow regimes, slug size and pressure drop. Chem Eng J 131:1–13. https://doi.org/10.1016/j.cej.2006.11.020
Kashid MN, Kiwiminsker L (2011) Quantitative prediction of flow patterns in liquid-liquid flow in micro-capillaries. Chem Eng Process 50:972–978. https://doi.org/10.1016/j.cep.2011.07.003
Kashid MN, Platte F, Agar DW, Turek S (2007) Computational modelling of slug flow in a capillary microreactor. J Comput Appl Math 203:487–497. https://doi.org/10.1016/j.cam.2006.04.010
Kashid MN, Rivas DF, Agar DW, Turek S (2008) On the hydrodynamics of liquid-liquid slug flow capillary microreactors. Asia-Pacific J Chem Eng 3:151–160. https://doi.org/10.1002/apj.127
Kashid MN, Renken A, Kiwi-Minsker L (2011a) Gas–liquid and liquid–liquid mass transfer in microstructured reactors. Chem Eng Sci 66:3876–3897. https://doi.org/10.1016/j.ces.2011.05.015
Kashid MN, Renken A, Kiwi-Minsker L (2011b) Influence of flow regime on mass transfer in different types of microchannels. Ind Eng Chem Res 50:6906–6914. https://doi.org/10.1021/ie102200j
Kinoshita H, Kaneda S, Fujii T, Oshima M (2007) Three-dimensional measurement and visualization of internal flow of a moving droplet using confocal micro-PIV. Lab Chip 7:338–346. https://doi.org/10.1039/b617391h
Lee SH, Min P, Park CG, Kim BH, Lee J, Choi SY (2014) Implantable micro-chip for controlled delivery of diclofenac sodium. J Control Release 196:52–59. https://doi.org/10.1016/j.jconrel.2014.09.019
Lee CY, Wang WT, Liu CC, Fu LM (2016) Passive mixers in microfluidic systems: a review. Chem Eng J 288:146–160. https://doi.org/10.1016/j.cej.2015.10.122
Lemenand T, Dupont P, Valle DD, Peerhossaini H (2013) Comparative efficiency of shear, elongation and turbulent droplet breakup mechanisms: review and application. Chem Eng Res Des 91:2587–2600. https://doi.org/10.1016/j.cherd.2013.03.017
Li Q, Angeli P (2017) Experimental and numerical hydrodynamic studies of ionic liquid-aqueous plug flow in small channels. Chem Eng J 328:717–736. https://doi.org/10.1016/j.cej.2017.07.037
Liu H, Zhang HY (2009) Droplet formation in a T-shaped microfluidic junction. J Appl Phys 106:034906. https://doi.org/10.1063/1.3187831
Liu C, Zhang Q, Zhu C, Fu T, Ma Y, Li HZ (2018) Formation of droplet and "string of sausages" for water-ionic liquid ([bmim][pf6]) two-phase flow in a flow-focusing device. Chem Eng Process Process Intensif 125:8–17. https://doi.org/10.1016/j.cep.2017.12.017
Madadelahi M, Shamloo A, Madadelahi M, Shamloo A (2017) Droplet-based flows in serpentine microchannels: chemical reactions and secondary flows Int. J Multiphase Flow 97:186–196. https://doi.org/10.1016/j.ijmultiphaseflow.2017.08.010
Mahdi Y, Daoud K, Tadrist L (2017) Two-phase flow patterns and size distribution of droplets in a microfluidic T-junction: experimental observations in the squeezing regime. C. R. Mecanique 345:259–270. https://doi.org/10.1016/j.crme.2017.02.001
Malsch D, Kielpinski M, Merthan R, Albert J, Mayer G, Kohler JM (2008) μ-PIV-Analysis of Taylor flow in micro channels. Chem Eng J 135:s166–s172. https://doi.org/10.1016/j.cej.2007.07.065
Mao ZS, Yang C (2017) Micro-mixing in chemical reactors: a perspective. Chin J Chem Eng 25:381–390. https://doi.org/10.1016/j.cjche.2016.09.012
Matsuoka A, Noishiki K, Mae K (2016) Experimental study of the contribution of liquid film for liquid-liquid taylor flow mass transfer in microchannel. Chem Eng Sci 155:306–313. https://doi.org/10.1016/j.ces.2016.08.021
Murphy TW, Zhang Q, Naler LB, Ma S, Lu C (2017) Recent advances in the use of microfluidic technologies for single cell analysis. Analyst 143:6–8. https://doi.org/10.1039/c7an01346a
Nonino C, Savino S, Giudice SD (2009) Numerical assessment of the mixing performance of different serpentine microchannels. Heat Trans Eng 30:101–112. https://doi.org/10.1080/01457630802293506
Oelgemöller M, Shvydkiv O (2011) Recent advances in microflow photochemistry. Molecules 16:7522–7550. https://doi.org/10.3390/molecules16097522
Özkan A, Erdem EY (2015) Numerical analysis of mixing performance in sinusoidal microchannels based on particle motion in droplets. Microfluid Nanofluid 19:1101–1108. https://doi.org/10.1007/s10404-015-1628-7
Plouffe P, Roberge DM, Macchi A (2016a) Liquid-liquid flow regimes and mass transfer in various micro-reactors. Chem Eng J 300:9–19. https://doi.org/10.1016/j.cej.2016.04.072
Plouffe P, Roberge DM, Sieber J, Bittel M, Macchi A (2016b) Liquid–liquid mass transfer in a serpentine micro-reactor using various solvents. Chem Eng J 285:605–615. https://doi.org/10.1016/j.cej.2015.09.115
Qian JY, Li XJ, Wu Z, Jin ZJ, Zhang JH, Sunden B (2019a) Slug formation analysis of liquid-liquid two-phase flow in T-junction microchannels. J Therm Sci Eng Appl 11(5):051017-8. https://doi.org/10.1115/1.4043385
Qian JY, Li XJ, Gao ZX, Jin ZJ (2019b) Mixing efficiency and pressure drop analysis of liquid-liquid two phases flow in serpentine microchannels. J Flow Chem. https://doi.org/10.1007/s41981-019-00040-1
Qian JY, Li XJ, Gao ZX, Jin ZJ (2019c) Mixing efficiency analysis on droplet formation process in microchannels by numerical methods. Processes 7:33. https://doi.org/10.3390/pr7010033
Qiu D, Silva LJ, Tonkovich AL, Arora R (2010) Micro-droplet formation in non-Newtonian fluid in a microchannel. Microfluid Nanofluid 8:531–548. https://doi.org/10.1007/s10404-009-0487-5
Raimondi NDM, Prat L, Gourdon C, Tasselli J (2014) Experiments of mass transfer with liquid-liquid slug flow in square microchannels. Chem Eng Sci 105:169–178. https://doi.org/10.1016/j.ces.2013.11.009
Raj R, Mathur N, Buwa VV (2010) Numerical simulations of liquid-liquid flows in microchannels. Ind Eng Chem Res 49:10606–10614. https://doi.org/10.1021/ie100626a
Sahu A, Vir AB, Molleti LNS, Ramji S, Pushpavanam S (2016) Comparison of liquid-liquid extraction in batch systems and microchannels. Chem Eng Process Process Intensif 104:190–200. https://doi.org/10.1016/j.cep.2016.03.010

Šalić A, Tušek A, Zelić B (2012) Application of microreactors in medicine and biomedicine. J Appl Biomed 10:137–153. https://doi.org/10.2478/v10136-012-0011-1

Salim A, Fourar M, Pironon J, Sausse J (2008) Oil–water two-phase flow in microchannels: flow patterns and pressure drop measurements. Can J Chem Eng 86:978–988. https://doi.org/10.1002/cjce.20108

Sang L, Hong Y, Wang F (2009) Investigation of viscosity effect on droplet formation in T-shaped microchannels by numerical and analytical methods. Microfluid Nanofluid 6:621–635. https://doi.org/10.1007/s10404-008-0329-x

Sarkar PS, Singh KK, Shenoy KT, Sinha A, Rao H, Ghosh SK (2012) Liquid–liquid two-phase flow patterns in a serpentine microchannel. Ind Eng Chem Res 51:5056–5066. https://doi.org/10.1021/ie201590f

Sattari-Najafabadi M, Esfahany MN, Wu Z, Sundén B (2017a) Hydrodynamics and mass transfer in liquid-liquid non-circular microchannels: comparison of two aspect ratios and three junction structures. Chem Eng J 322:328–338. https://doi.org/10.1016/j.cej.2017.04.028

Sattari-Najafabadi M, Esfahany N, Wu Z, Sundén B (2017b) The effect of the size of square microchannels on hydrodynamics and mass transfer during liquid-liquid slug flow. AIChE J 63:5019–5028. https://doi.org/10.1002/aic.15822

Sattari-Najafabadi M, Esfahany MN, Wu Z, Sunden B (2018) Mass transfer between phases in microchannels: a review. Chem Eng Process Process Intensif 127:213–237. https://doi.org/10.1016/j.cep.2018.03.012

Seemann R, Brinkmann M, Pfohl T, Herminghaus S (2012) Droplet based microfluidics. Rep Prog Phys 75:016601. https://doi.org/10.1088/0034-4885/75/1/016601

Shui L, Eijkel JC, Van dBA (2007) Multiphase flow in microfluidic systems –control and applications of droplets and interfaces. Adv Colloid Interface Sci 13:35–49. https://doi.org/10.1016/j.cis.2007.03.001

Song H, Chen DL, Ismagilov RF (2006) Reactions in droplets in microfluidic channels. Angew Chem Int Ed 45:7336–7356. https://doi.org/10.1002/anie.200601554

Teh SY, Lin R, Hung LH, Lee AP (2008) Droplet microfluidics. Lab Chip 8:198–220. https://doi.org/10.1039/b715524g

Tice JD, Song H, Lyon AA, Ismagilov RF (2003) Formation of droplets and mixing in multiphase microfluidics at low values of the reynolds and the capillary numbers. Langmuir 19:9127–9133. https://doi.org/10.1021/la030090w

Timung S, Tiwari V, Singh AK, Mandal TK, Bandyopadhyay D (2015) Capillary force mediated flow-patterns and non-monotonic pressure drop characteristics of oil-water microflows. Can J Chem Eng 93:1736–1743. https://doi.org/10.1002/cjce.22273

Tsaoulidis D, Angeli P (2016) Effect of channel size on liquid-liquid plug flow in small channels. AIChE J 62:315–324. https://doi.org/10.1002/aic.15026

Tsaoulidis D, Dore V, Angeli P, Plechkova NV, Seddon KR (2013) Flow patterns and pressure drop of ionic liquid-water two-phase flows in microchannels. Int J Multiphase Flow 54:1–10. https://doi.org/10.1016/j.ijmultiphaseflow.2013.02.002

Van Loo S, Stoukatch S, Kraft M, Gilet T (2016) Droplet formation by squeezing in a microfluidic cross-junction. Microfluid Nanofluid 20:146. https://doi.org/10.1007/s10404-016-1807-1

Vladisavljevic GT, Kobayashi I, Nakajima M (2012) Production of uniform droplets using membrane, microchannel and microfluidic emulsification devices. Microfluid Nanofluid 13:151–178. https://doi.org/10.1007/s10404-012-0948-0

Wang K, Luo G (2017) Microflow extraction: a review of recent development. Chem Eng Sci 169:18–33. https://doi.org/10.1016/j.ces.2016.10.025

Wang W, Liu Z, Jin Y, Cheng Y (2011) LBM simulation of droplet formation in micro-channels. Chem Eng J 173:828–836. https://doi.org/10.1016/j.cej.2011.08.040

Wang J, Wang J, Feng L, Lin T (2015) Fluid mixing in droplet-based microfluidics with a serpentine microchannel. Rsc Advances 5:104138–104144. https://doi.org/10.1039/c5ra21181f

Ward K, Fan ZH (2015) Mixing in microfluidic devices and enhancement methods. J Micromech Microeng 25:094001. https://doi.org/10.1088/0960-1317/25/9/0940

Wehking JD, Gabany M, Chew L, Kumar R (2014) Effects of viscosity, interfacial tension, and flow geometry on droplet formation in a microfluidic T-junction. Microfluid Nanofluid 16:441–453. https://doi.org/10.1007/s10404-013-1239-0

Woitalka A, Kuhn S, Jensen KF (2014) Scalability of mass transfer in liquid-liquid flow. Chem Eng Sci 116:1–8. https://doi.org/10.1016/j.ces.2014.04.036

Wu L, Liu X, Zhao Y, Chen Y (2017) Role of local geometry on droplet formation in axisymmetric microfluidics. Chem Eng Sci 163:56–67. https://doi.org/10.1016/j.ces.2017.01.022

Xu J, Luo G, Li S, Chen GG (2006) Shear force induced monodispersed droplet formation in a microfluidic device by controlling wetting properties. Lab Chip 6:131–136. https://doi.org/10.1039/b509939k

Xu J, Li S, Tan J, Luo G (2008) Correlations of droplet formation in T-junction microfluidic devices: from squeezing to dripping. Microfluid Nanofluid 5:711–717. https://doi.org/10.1007/s10404-008-0306-4

Xu B, Cai W, Liu X, Zhang X (2013) Mass transfer behavior of liquid–liquid slug flow in circular cross-section microchannel. Chem Eng Res Des 91:1203–1211. https://doi.org/10.1016/j.cherd.2013.01.0

Yagodnitsyna AA, Kovalev AV, Bilsky AV (2016) Flow patterns of immiscible liquid-liquid flow in a rectangular microchannel with T-junction. Chem Eng J 303:547–554. https://doi.org/10.1016/j.cej.2016.06.023

Yang L, Li S, Liua J, Cheng J (2018) Fluid mixing in droplet-based microfluidics with T junction and convergent-divergent sinusoidal microchannels. Electrophoresis 39:512–520. https://doi.org/10.1002/elps.201700374

Yao X, Zhang Y, Du L, Liu J, Yao J (2015) Review of the applications of microreactors. Renew Sust Energ Rev 47:519–539. https://doi.org/10.1016/j.rser.2015.03.078

Yao C, Zhao Y, Chen G (2018) Multiphase processes with ionic liquids in microreactors: hydrodynamics, mass transfer and applications. Chem Eng Sci 189:340–359. https://doi.org/10.1016/j.ces.2018.06.007

Yue J (2018) Multiphase flow processing in microreactors combined with heterogeneous catalysis for efficient and sustainable chemical synthesis. Catal Today 308:3–19. https://doi.org/10.1016/j.cattod.2017.09.041

Yun SH, Sang JJ, Lee EZ, Park HS, Hong WH (2011) Microfluidic extraction using two phase laminar flow for chemical and biological applications. Korean J Chem Eng 28:633–642. https://doi.org/10.1007/s11814-010-0533-8

Zhang Y, Zhang X, Xu B, Cai W, Wang F (2016) CFD simulation of mass transfer intensified by chemical reactions in slug flow microchannels. Can J Chem Eng 93:2307–2314. https://doi.org/10.1002/cjce.22360

Zhang Q, Liu H, Zhao S, Yao C, Chen G (2019) Hydrodynamics and mass transfer characteristics of liquid–liquid slug flow in microchannels: The effects of temperature, fluid properties and channel size. Chem Eng J 358:794–805. https://doi.org/10.1016/j.cej.2018.10.056

Zhao Y, Chen G, Yuan Q (2006) Liquid–liquid two-phase flow patterns in a rectangular microchannel. AIChE J 52:4052–4060. https://doi.org/10.1002/aic.11029

Zhao Y, Chen G, Yuan Q (2007) Liquid-liquid two-phase mass transfer in the T-junction microchannels. AIChE J 53:3042–3053. https://doi.org/10.1002/aic.11333

Zhao Y, Su Y, Chen G, Quan Y (2010) Effect of surface properties on the flow characteristics and mass transfer performance in microchannels. Chem Eng Sci 65:1563–1570. https://doi.org/10.1016/j.ces.2009.10.027

Zhao S, Wang W, Zhang M, Shao T, Jin Y, Cheng Y (2012) Three-dimensional simulation of mixing performance inside droplets in micro-channels by lattice boltzmann method. Chem Eng J 207–208:267–277. https://doi.org/10.1016/j.cej.2012.06.098

Zhao Y, Cheng Y, Shang L, Wang J, Xie Z, Gu Z (2015a) Microfluidic synthesis of barcode particles for multiplex assays. Small 11:151–174. https://doi.org/10.1002/smll.201401600

Zhao S, Riaud A, Luo G, Jin Y, Cheng Y (2015b) Simulation of liquid mixing inside micro-droplets by a lattice boltzmann method. Chem Eng Sci 131:118–128. https://doi.org/10.1016/j.ces.2015.03.066

Zheng N, Zhou M, Du C, Wang S, Lu W (2013) 5-fluorouracil delivery from a novel three-dimensional micro-device: in vitro and in vivo evaluation. Arch Pharm Res 36:1487–1493. https://doi.org/10.1007/s12272-013-0168-5

Zhu P, Wang L (2017) Passive and active droplet generation with microfluidics: a review. Lab Chip 17:34–75. https://doi.org/10.1039/c6lc01018k